

Comparison of Nuclear Starburst Luminosities between Seyfert 1 and 2 Galaxies Based on Near-infrared Spectroscopy

Masatoshi Imanishi^{1,2} and Keiichi Wada¹

National Astronomical Observatory, 2-21-1, Osawa, Mitaka, Tokyo 181-8588, Japan

imanishi@optik.mtk.nao.ac.jp, wada.keiichi@nao.ac.jp

ABSTRACT

We report on infrared K - (2–2.5 μm) and L -band (2.8–4.1 μm) slit spectroscopy of 23 Seyfert 1 galaxies in the CfA and 12 μm samples. A polycyclic aromatic hydrocarbon (PAH) emission feature at 3.3 μm in the L band is primarily used to investigate nuclear star-forming activity in these galaxies. The 3.3 μm PAH emission is detected in 10 sources (=43%), demonstrating that detection of nuclear star-formation in a significant fraction of Seyfert 1 galaxies is now feasible. For the PAH-detected nuclei, the surface brightness values of the PAH emission are as high as those of typical starbursts, suggesting that the PAH emission probes the putative nuclear starbursts in the dusty tori around the central active galactic nuclei (AGNs). The magnitudes of the nuclear starbursts are quantitatively estimated from the observed 3.3 μm PAH emission luminosities. The estimated starburst luminosities relative to some indicators of AGN powers in these Seyfert 1s are compared with 32 Seyfert 2s in the same samples that we have previously observed. We find that there is no significant difference in nuclear starburst to AGN luminosity ratios between Seyfert 1 and 2 galaxies, and that nuclear starburst luminosity positively correlates with AGN power in both types of Seyferts. Our results favor a *slightly-modified* AGN unification model, which predicts that nuclear starbursts occurring in the dusty tori of Seyferts are physically connected to the central AGNs, rather than the *classical* unification

¹Visiting Astronomer at the Infrared Telescope Facility, which is operated by the University of Hawaii under Cooperative Agreement no. NCC 5-538 with the National Aeronautics and Space Administration, Office of Space Science, Planetary Astronomy Program.

²Based in part on data collected at Subaru Telescope, which is operated by the National Astronomical Observatory of Japan.

paradigm, in which the dusty tori simply hide the central AGNs of Seyfert 2s and reprocess AGN radiation as infrared dust emission in Seyferts. No significant differences in nuclear star formation properties are recognizable between Seyfert 1s in the CfA and 12 μm samples.

Subject headings: galaxies: active — galaxies: nuclei — galaxies: Seyfert — infrared: galaxies

1. Introduction

Seyfert galaxies constitute a population that shows bright optical nuclei (Seyfert 1943), and the most numerous class of active galactic nuclei (AGNs) in the local universe. It is generally believed that they contain a mass-accreting supermassive black hole as a central engine, which is surrounded by toroidally distributed dust and molecular gas (the so-called “dusty torus”). There are two types of Seyfert galaxy, type-1 (which show broad optical emission lines) and type-2 (which do not). The different emission properties are explained by the AGN unification paradigm, in which the central engine of a Seyfert 2 galaxy is intrinsically the same as that in a Seyfert 1 galaxy, but is obscured from our line-of-sight by a dusty torus (Antonucci 1993). In this *classical* AGN unification paradigm, intrinsic torus properties are assumed to be the same for the two types of Seyfert galaxy, and the primary role of the dusty tori is twofold: they simply (1) hide the central AGNs in Seyfert 2 galaxies, and (2) absorb AGN radiation and re-radiate as infrared dust emission in both Seyfert 1 and 2 galaxies (Pier & Krolik 1992).

Since a dusty torus is rich in molecular gas, *nuclear* starbursts may occur there, and energy feedback from the nuclear starbursts could work to inflate the torus (Fabian et al. 1998). Using high-resolution three-dimensional hydrodynamic simulations, Wada & Norman (2002) showed that the nuclear starbursts in an extended (tens of pc) dusty torus can produce an inflated, turbulent torus around a central supermassive black hole. They also suggested the possibility that the nuclear starbursts in the torus may be more powerful in Seyfert 2s than in Seyfert 1s, because in a more inflated torus with stronger nuclear starbursts, the chance that the central engine is obscured and that, therefore, the galaxy would be classified as a Seyfert 2, would be higher. From a study of the equivalent width of the iron K α emission at 6.4 keV in X-rays, Levenson et al. (2002) made a similar suggestion. To obtain a deeper understanding of AGNs, it is important to observationally constrain the putative nuclear starbursts in the dusty tori of Seyferts, and to test whether this *slightly-modified* AGN model (with nuclear starbursts in the dusty tori) is more representative of actual AGNs than the *classical* model.

Some observations and simple theoretical considerations of gravitational instability suggest that nuclear starbursts in Seyfert galaxies are likely to occur at the outer part of the dusty torus (Heckman et al. 1997; Imanishi 2003). Attempts have been made to detect nuclear starbursts in the tori of Seyfert galaxies by several groups in the UV-optical (Gonzalez Delgado et al. 2001) and near-infrared at $\lambda < 2.5 \mu\text{m}$ (Oliva et al. 1999). Detection has been successful only in type-2 sources, because unattenuated AGN emission from Seyfert 1 galaxies weakens the signatures of the nuclear starbursts in the observed spectra and makes their detection difficult; however, it is also possible that Seyfert 1s have weaker nuclear starbursts than do Seyfert 2s (Wada & Norman 2002). Until very recently, very little about nuclear starbursts in Seyfert 1 galaxies has been constrained observationally.

To study nuclear starbursts in Seyfert galaxies, infrared *L*-band ($2.8\text{--}4.1 \mu\text{m}$) spectroscopy can be a very powerful tool, as stated by Imanishi (2002). First, a starburst usually shows a strong polycyclic aromatic hydrocarbon (PAH) emission feature at $3.3 \mu\text{m}$, whereas a pure AGN shows only a featureless continuum, with virtually no PAH emission. Thus, from an *L*-band spectrum, we can estimate the fractional contribution from a starburst and an AGN to the observed flux (Imanishi & Dudley 2000). Second, the $3.3 \mu\text{m}$ PAH emission feature is intrinsically so strong that even a weak starburst is detectable (Imanishi 2002). In fact, weak starbursts that had previously been undetected with other methods have been newly found in some Seyfert 2 galaxies (Imanishi 2002). Third, dust extinction is much lower in the *L*-band ($A_L/A_V \sim 0.06$; Rieke & Lebofsky 1985) than at shorter wavelengths, so that differences in the bright AGN glare emission of Seyfert 1s and 2s caused by the flux attenuation by the dusty torus are significantly reduced, as compared to shorter wavelengths. This suggests that, given the success of the detection of nuclear starbursts in a significant fraction of Seyfert 2 galaxies (Imanishi 2002, 2003), similar detection may also be feasible in many Seyfert 1 galaxies. This expectation has actually been confirmed by the successful detection of nuclear starbursts in a few type-1 Seyferts (Rodriguez-Ardila & Viegas 2003). Finally, it has been proven that nuclear starbursts in the tori of Seyfert galaxies are reasonably quantifiable from observed $3.3 \mu\text{m}$ PAH emission luminosities, owing mainly to the low dust extinction in the *L*-band (Imanishi 2002). All of these advantages make *L*-band spectroscopy an excellent tool to quantitatively determine nuclear starburst luminosities in Seyfert galaxies, and to compare the starburst luminosities in Seyfert 1 and 2 galaxies.

Besides *L*-band spectra, *K*-band ($2\text{--}2.5 \mu\text{m}$) spectra can also be used to study stellar emission in Seyfert nuclei. Since the CO absorption features at $\lambda_{\text{rest}} = 2.3\text{--}2.4 \mu\text{m}$ in the rest-frame are produced by stars, and not by a pure AGN, emission from stars and AGNs is distinguishable using these features (Oliva et al. 1999; Ivanov et al. 2000; Imanishi & Alonso-Herrero 2004). Furthermore, nuclear $K - L$ colors provide useful information on the origin of nuclear emission from Seyfert galaxies (Alonso-Herrero et al. 2003; Willner et al.

1984). A combination of L - and K -band spectra can add further constraints on the nuclear emission properties in Seyfert galaxies.

We have extensively studied nuclear starbursts in Seyfert 2 galaxies through L - and K -band spectroscopy (Imanishi 2003; Imanishi & Alonso-Herrero 2004). In this paper, we report the results of L - and K -band spectroscopy of Seyfert 1 galaxies, to compare with the data for Seyfert 2 galaxies. Throughout the paper, $H_0 = 75 \text{ km s}^{-1} \text{ Mpc}^{-1}$, $\Omega_M = 0.3$, and $\Omega_\Lambda = 0.7$ are adopted.

2. Targets

The Seyfert 2 galaxies previously studied by Imanishi (2003) and Imanishi & Alonso-Herrero (2004) were taken from the CfA (Huchra & Burg 1992) and 12 μm (Rush, Malkan, & Spinoglio 1993) samples. The CfA and 12 μm samples were selected through optical spectroscopy of large numbers of galaxies limited by optical and *IRAS* 12 μm fluxes, respectively, and are thought not to be strongly biased toward or against the presence of nuclear starbursts in the torus. Our aim is to investigate the emission properties of the *nuclear* starbursts in the torus, rather than more powerful *circumnuclear* starbursts in host galaxies, which are often ring-shaped at $\sim\text{kpc}$ scale from the center (Storchi-Bergmann, Wilson, & Baldwin 1996). Since we make the investigation through ground-based spectroscopy using a 1–2 arcsec wide slit, Seyfert 1 galaxies at $z=0.008\text{--}0.035$ are selected as the targets in the same way as the Seyfert 2 galaxies used for comparison (see Imanishi 2003), where 1 arcsec corresponds to a physical scale of 150 pc ($z = 0.008$) to 650 pc ($z = 0.035$). To be best observable from Mauna Kea, Hawaii (our observing site), the declinations of Seyfert 1 galaxies are limited to being larger than -30° . Owing to the telescope limit of the IRTF 3 m telescope that was mainly used in this study, a restriction of declination of $<68^\circ$ is also applied. These selection criteria result in 14 and 22 Seyfert 1 galaxies in the CfA and 12 μm samples, respectively. Of these, six sources are included in both samples, totaling 30 Seyfert 1 galaxies. Two Seyfert 1 galaxies, NGC 4253 and Mrk 1239, had L -band spectra available at the time of our observations (Rodriguez-Ardila & Viegas 2003). Five Seyfert 1 galaxies (NGC 3080, Mrk 789, NGC 6104, MCG-3-7-11, and NGC 4602) could not be observed owing to our limited telescope time. We observed the remaining 23 sources. Detailed information on the observed 25 Seyfert 1 galaxies (23 sources by ourselves and 2 sources by Rodriguez-Ardila & Viegas) is summarized in Table 1. The infrared luminosities of the majority of them are $<10^{11}L_\odot$, with the highest one with $\sim 10^{11.5}L_\odot$ (NGC 7469), so that the observed targets are moderately infrared luminous Seyfert 1s, with no ultraluminous infrared galaxies ($L_{\text{IR}} > 10^{12}L_\odot$; Sanders & Mirabel 1996) included. There are no obvious biases in the 25

objects selected, and so the observed sample is large enough and relatively unbiased such as to be nearly statistically complete. Thus, these datasets provide important information on nuclear starbursts in Seyfert 1 galaxies.

3. Observations

All observations were made with the SpeX (Rayner et al. 2003) at the IRTF 3 m telescope on Mauna Kea, Hawaii, with the exception of NGC 7469, which was observed with IRCS (Kobayashi et al. 2000) at the Subaru 8.2 m telescope at Mauna Kea. Table 2 tabulates the detailed information on these observing runs.

For the IRTF SpeX observing runs, the 1.9–4.2 μm cross-dispersed mode with a 1''.6 wide slit was employed. This mode enables L - (2.8–4.1 μm) and K -band (2–2.5 μm) spectra to be obtained simultaneously, with a spectral resolution of $R \sim 500$. The sky conditions were photometric throughout the observations, and the seeing sizes at K were in the range 0''.4–1''.0 (full-width at half-maximum; FWHM). The position angle of the slit was set along the north-south direction. A standard telescope nodding technique (ABBA pattern) with a throw of 7.5 arcsec was employed along the slit to subtract background emission. The telescope tracking was monitored with the infrared slit-viewer of SpeX. Each exposure was 15 sec, and 2 coadds were made at each position.

The Subaru IRCS observation of NGC 7469 was made using a 0''.9-wide slit, and with a 58-mas pixel scale. The achievable spectral resolution at 3.5 μm was $R \sim 140$. The seeing at K was $\sim 0''.7$ in FWHM. The weather was not photometric, owing to the presence of cirrus. A standard telescope nodding technique (ABBA pattern), with a throw of 7 arcsec along the slit, was employed. Each exposure was 2.5 sec, and 15 coadds were made at each position.

F- and G-type main sequence stars (Table 2) were observed as standard stars, with airmass difference of < 0.1 to the individual Seyfert 1 nuclei, to correct for the transmission of the Earth’s atmosphere. The K - and L -band magnitudes of the standard stars were estimated from their V -band (0.6 μm) magnitudes, adopting the $V - K$ and $V - L$ colors appropriate to the stellar types of individual standard stars, respectively (Tokunaga 2000).

Standard data reduction procedures were employed using IRAF¹, in the same way as employed for Seyfert 2 galaxies (Imanishi 2003). Initially, bad pixels and pixels hit by cosmic

¹IRAF is distributed by the National Optical Astronomy Observatories, operated by the Association of Universities for Research in Astronomy, Inc. (AURA), under cooperative agreement with the National Science Foundation.

rays were replaced with the interpolated values of the surrounding pixels. Then, frames taken with an A (or B) beam were subtracted from frames subsequently taken with a B (or A) beam, and the resulting subtracted frames were added and divided by a spectroscopic flat image. The spectral extraction of Seyfert 1 galaxies and standard stars along the slit was then made by integrating signals over $2''.1$ – $3''.0$ for the IRTF SpeX data and $1''.1$ for the Subaru IRCS data. Wavelength calibration was performed using the wavelength-dependent transmission of the Earth’s atmosphere. The Seyfert 1 spectra were divided by those of the corresponding standard stars, and were multiplied by the spectra of blackbodies with temperatures corresponding to those of the individual standard stars (Table 2). Appropriate spectral binning was applied for faint sources. Flux calibration was made using signals detected inside our slit spectra, with the exception of NGC 7469, the flux calibration of which was made using a previous photometric measurement ($L = 8.36$ mag; $1''.4$ aperture) by Marco & Alloin (1998).

4. Results

4.1. *L*-band

Figure 1 presents flux-calibrated *L*-band slit spectra of the 23 Seyfert 1 nuclei. Since the nuclear *L*-band emission from Seyfert 1 galaxies is often dominated by compact, spatially-unresolved emission (Alonso-Herrero et al. 1998, 2003), nuclear *L*-band fluxes measured with slightly different apertures should, in principle, be similar. In fact, flux levels based on our slit spectra are in reasonable agreement (mostly <0.5 mag) with previous photometric measurements using <5 arcsec apertures, suggesting that possible flux loss in our slit spectra will not significantly affect emission flux estimates.

Many sources show clear excess at the expected wavelength of the $3.3\text{ }\mu\text{m}$ PAH emission feature at $(1 + z) \times 3.29\text{ }\mu\text{m}$. When at least two successive data points are significantly higher than an adopted continuum level, we regard the $3.3\text{ }\mu\text{m}$ PAH emission feature as detected. Using this criterion, $3.3\text{ }\mu\text{m}$ PAH emission is detected in 10 Seyfert 1 nuclei, marked with “ $3.3\text{ }\mu\text{m}$ PAH” in Fig. 1. The fluxes, luminosities, and rest-frame equivalent widths ($\text{EW}_{3.3\text{PAH}}$) of the $3.3\text{ }\mu\text{m}$ PAH emission are estimated using the method described by Imanishi (2002) and are summarized in Table 3.

Although PAH emission from nuclear star-formation is detected in $\sim 43\%$ ($=10/23$) of the observed Seyfert 1 nuclei, the significantly smaller $\text{EW}_{3.3\text{PAH}}$ values, as compared to star-formation (~ 100 nm; Imanishi & Dudley 2000), suggest that a featureless continuum from hot dust heated by AGNs contributes dominantly to the observed *L*-band fluxes, and

dilutes the $3.3 \mu\text{m}$ PAH emission. To estimate the energetic importance of the detected nuclear star formation to the total luminosities of these Seyfert 1 galaxies, we investigate the nuclear $3.3 \mu\text{m}$ PAH to infrared luminosity ratios ($L_{\text{nuclear-3.3PAH}}/L_{\text{IR}}$), as we did for Seyfert 2 galaxies (Imanishi 2002, 2003). The $L_{\text{nuclear-3.3PAH}}/L_{\text{IR}}$ ratios in these Seyfert 1 galaxies are summarized in column 5 of Table 3. As was the case for Seyfert 2 galaxies in the CfA and $12 \mu\text{m}$ samples (Imanishi 2003), the ratios in Seyfert 1 galaxies are also much smaller than those of star-formation dominated galaxies ($\sim 10^{-3}$; Mouri et al. 1990; Imanishi 2002). This suggests that the detected nuclear star-formation contributes little to the total infrared luminosities of these Seyfert 1 galaxies, which should be dominated by AGNs and/or extended star-formation in host galaxies.

4.2. *K*-band

For sources observed with the IRTF SpeX, *K*-band spectra are also available. Figure 2 shows flux-calibrated *K*-band slit spectra of 22 sources, with the exception of NGC 7469.

4.2.1. *K* – *L* Colors

Since the SpeX *K*- and *L*-band spectra were obtained simultaneously, possible slit loss should be at a similar level. Thus, $K - L$ colors should be less uncertain than the absolute *K*- or *L*-band magnitudes themselves. Table 4 summarizes the nuclear $K - L$ colors measured with our slit spectra.

The majority of the observed Seyfert 1 galaxies show $K - L = 1\text{--}2$ mag, which is similar to the intrinsic AGN colors of Seyfert 1 galaxies (Alonso-Herrero et al. 2003), but much redder than those of star-formation ($K - L < 0.4$; Willner et al. 1984). This suggests that the *K*- and *L*-band emission from Seyfert 1 nuclei detected inside our slit spectra come largely from AGN-originated emission.

4.2.2. Emission Lines

The Br γ ($\lambda_{\text{rest}} = 2.166 \mu\text{m}$) emission lines are discernible in the spectra of several sources. The line widths of the Br γ emission in Seyfert 1 galaxies are so broad that the Br γ fluxes are reasonably quantifiable from our moderate-resolution ($R \sim 500$) spectra. For Seyfert 1 galaxies with clear Br γ detection, we fit the Br γ emission lines with Gaussian profiles, which are shown as solid lines in Figure 2. The derived FWHMs, fluxes, luminosities, and

rest-frame equivalent widths of the Br γ emission lines are summarized in Table 5.

Besides the Br γ emission lines, there are possible signs of narrow (<500 km s $^{-1}$ in FWHM) emission lines, such as H₂ 1–0 S(1) at $\lambda_{\text{rest}} = 2.12$ μm , in some sources. To discuss these narrow emission lines in a quantitatively reliable manner, by tracing their profiles, spectral-resolution of $R > 1000$ is desirable. No quantitative estimates for narrow emission lines are made in our lower resolution ($R \sim 500$) spectra.

4.2.3. CO Absorption Features

Some sources show flux depression at $\lambda_{\text{rest}} > 2.3$ μm , as compared to shorter wavelengths. This is usually attributed to CO absorption at 2.3–2.4 μm , caused by stars. To estimate its strength, we adopt the spectroscopic CO index proposed by Doyon, Joseph, & Wright (1994). This index is defined as

$$\text{CO}_{\text{spec}} \equiv -2.5 \log < R_{2.36} >, \quad (1)$$

where $< R_{2.36} >$ is the average of actual signals at $\lambda_{\text{rest}} = 2.31$ –2.40 μm divided by a power-law continuum ($F_\lambda = \alpha \times \lambda^\beta$) extrapolated from shorter wavelengths. In our spectra, data points at $\lambda_{\text{rest}} = 2.1$ –2.29 μm , excluding clear emission lines, are used to determine a continuum level, because this wavelength range is fully covered in the $\lambda_{\text{obs}} = 2.07$ –2.5 μm (observed frame) spectra. Although this wavelength range is slightly different from that employed by Doyon et al. ($\lambda_{\text{rest}} = 2.0$ –2.29 μm), our spectroscopic CO index is essentially the same as theirs. For sources with clear CO absorption signatures, the adopted continuum levels are shown as dashed lines in Figure 2 and the derived CO indices are summarized in Table 6.

Even for the detected sources, with the exception of NGC 2639, the CO absorption feature is weak. The major uncertainty of the CO index comes from the ambiguity of the continuum determination, which is difficult to assess quantitatively. For other sources without signatures of the absorption, we simply regard the CO absorption as undetected.

Correction of the observed spectroscopic CO index for the dilution by AGNs' featureless continuum in the K -band could, in principle, enable us to investigate nuclear star-formation properties in more detail, as has been undertaken in Seyfert 2 galaxies (Ivanov et al. 2000; Imanishi & Alonso-Herrero 2004). However, for this correction process to work reasonably well, the observed spectroscopic CO index must be >0.1 . In Seyfert 1 galaxies, the observed CO absorption feature is usually much shallower than in Seyfert 2 galaxies, owing to a higher contribution from unattenuated AGNs' featureless continuum in the former. Thus, no correction of the observed spectroscopic CO index for AGNs' dilution is attempted.

NGC 2639 is an exception; its observed spectroscopic CO index, without any AGN correction, is as large as those found in many star-forming galaxies (Coziol, Doyon, & Demers 2001). The $K - L$ color of this source is unusually blue as compared to the other Seyfert 1 galaxies in our sample (Table 4). The contribution from nuclear star-formation to the observed K -band flux must be high in this Seyfert 1 galaxy.

5. Discussion

5.1. Origins of the Detected Stellar Emission

The nuclear K - and L -band fluxes from Seyfert 1 galaxies are the superposition of emission from (1) the AGN, (2) putative nuclear starbursts in the dusty torus, (3) the central part of old bulge stars, and (4) the central part of disk stars. The $3.3 \mu\text{m}$ PAH emission can, in principle, originate in the latter three components. Nuclear starbursts and quiescent bulge and disk star-formation can be distinguished, based on the emission surface brightness of star-forming activity.

Heckman (2001) estimated the star-formation rate per unit area of $10^{-1} \text{ M}_\odot \text{ yr}^{-1} \text{ kpc}^{-2}$ as a lower limit, beyond which the superwind activity, a characteristic property of starbursts, can occur. This limit corresponds to the infrared surface brightness of $S_{\text{IR}} \sim 2 \times 10^{42} \text{ ergs s}^{-1} \text{ kpc}^{-2}$ (Kennicutt 1998), or to the $3.3 \mu\text{m}$ PAH emission surface brightness of $S_{3.3\text{PAH}} \sim 2 \times 10^{39} \text{ ergs s}^{-1} \text{ kpc}^{-2}$ (Imanishi 2002). The $3.3 \mu\text{m}$ PAH surface brightness values in the observed Seyfert 1 galaxies are summarized in the last column of Table 3. At least for the PAH-detected Seyfert 1 nuclei, the surface brightness values of the $3.3 \mu\text{m}$ PAH emission are as high as those typically found in starbursts. We therefore conclude that the detected $3.3 \mu\text{m}$ PAH emission probes putative nuclear starbursts in the dusty torus, rather than quiescent star-formation. For the PAH-undetected sources, the upper limits of the surface brightness are also substantially above the threshold.

For Seyfert 2 galaxies in the CfA and $12 \mu\text{m}$ samples, Imanishi & Alonso-Herrero (2004) drew the same conclusion, based on the same calculation, that the detected $3.3 \mu\text{m}$ PAH emission should come from nuclear starbursts in the dusty tori. Thus, we can use the $3.3 \mu\text{m}$ PAH emission as a useful probe for nuclear starbursts in both Seyfert 1 and 2 galaxies.

5.2. Comparison of Nuclear Starburst Luminosities between Seyfert 1s and 2s

Imanishi (2002, 2003) showed that the luminosities of the nuclear starbursts in *Seyfert*

$2s$ are reasonably quantifiable from the *observed* $3.3\text{ }\mu\text{m}$ PAH emission luminosities inside slit spectra, primarily because (1) dust extinction is low at $3\text{--}4\text{ }\mu\text{m}$, and (2) the nuclear starbursts are thought to occur at the outer part of the dusty torus, where obscuration is expected not to be severe. Thus, we can make the reasonable assumption that the nuclear starburst luminosities in *Seyfert 1s* are also quantitatively determined, with reasonable accuracy, from the observed $3.3\text{ }\mu\text{m}$ PAH emission luminosities.

To compare nuclear starburst luminosities between Seyfert 1s and 2s, we normalize the luminosities with AGN powers. In both the classical and slightly-modified AGN unification models, the AGN-powered infrared emission should be more highly-attenuated in Seyfert 2s than in Seyfert 1s, owing to higher obscuration by the dusty tori in the former. However, a comparison of infrared spectral energy distributions between Seyfert 1s and 2s has suggested that the obscuring effects for the AGN emission from moderately infrared luminous Seyfert 2s, except the most infrared luminous ($L_{\text{IR}} > 10^{12}L_{\odot}$) and dustiest ones (i.e., ultraluminous infrared galaxies), becomes insignificant at $>10\text{ }\mu\text{m}$ (Alonso-Herrero et al. 2003). Since no Seyfert 2s studied by Imanishi (2003) have $L_{\text{IR}} > 10^{12}L_{\odot}$, we first use the *IRAS* $12\text{ }\mu\text{m}$ and $25\text{ }\mu\text{m}$, and ground-based *N*-band ($10.6\text{ }\mu\text{m}$) luminosities, because these luminosities have been argued to be good tracers of AGN powers in Seyfert galaxies, with less contamination from host galaxies' emission than *IRAS* $60\text{ }\mu\text{m}$ and $100\text{ }\mu\text{m}$ luminosities (Spinoglio & Malkan 1989; Rodriguez Espinosa & Perez Garcia 1997; Alonso-Herrero et al. 2002).

Figures 3a, 3b, and 3c compare the *IRAS* $12\text{ }\mu\text{m}$ luminosities, *IRAS* $25\text{ }\mu\text{m}$ luminosities, and *N*-band luminosities measured with $>4''$ apertures using single-pixel detectors from the ground, with the observed nuclear $3.3\text{ }\mu\text{m}$ PAH emission luminosities through our slit spectroscopy. Both Seyfert 1s (this paper) and 2s (Imanishi 2003) are plotted. The abscissa and ordinate are taken to trace the powers of the AGNs and nuclear starbursts, respectively (Imanishi 2002, 2003). If Seyfert 2s have intrinsically stronger nuclear starbursts in the dusty tori, then their distribution should be to the upper-left side of that of Seyfert 1s. However, no significant difference is evident in the distribution of Seyfert 1s and 2s. Both Seyfert 1s and 2s follow similar $3.3\text{ }\mu\text{m}$ PAH to $12\text{ }\mu\text{m}$, $25\text{ }\mu\text{m}$, and *N*-band luminosity ratios within the scatters. The distribution of the absolute luminosities of the $3.3\text{ }\mu\text{m}$ PAH emission, $12\text{ }\mu\text{m}$, $25\text{ }\mu\text{m}$, and *N*-band is also similar in Seyfert 1s and 2s. Even if there were some degree of obscuration effect for the AGN emission from Seyfert 2s at $>10\text{ }\mu\text{m}$, correction would move the plots of *Seyfert 2s to the right* in these figures. In this case, the nuclear starburst to AGN luminosity ratios in Seyfert 2s would be even smaller, which is opposite to the predictions of Wada & Norman (2002).

In all the plots of Figs. 3a, 3b, and 3c, *IRAS* $12\text{ }\mu\text{m}$, *IRAS* $25\text{ }\mu\text{m}$, and *N*-band aperture ($>4''$) measurements, which were taken as good indicators of AGN powers, could contain

emission from star-formation in host galaxies, including the ring-shaped kpc-scale circumnuclear starbursts, if they exist. Maiolino et al. (1995) suggested that the host galaxies of Seyfert 2s are more luminous than those of Seyfert 1s. *IRAS* fluxes at longer wavelengths, such as 60 μm and 100 μm , may be severely contaminated by the host galaxies' emission. However, the contamination is expected to be minimal at *IRAS* 12 μm and 25 μm (Spinoglio & Malkan 1989; Rodriguez Espinosa & Perez Garcia 1997). If the host galaxies' contamination is significant, then correction for the stronger contamination in Seyfert 2s will move the plots of Seyfert 2s to the left, as compared to Seyfert 1s, so that the plots in Figs. 3a, 3b, and 3c is still consistent with the scenario of stronger nuclear starbursts in Seyfert 2s (Wada & Norman 2002).

This possible ambiguity can be minimized if N -band photometry of spatially-unresolved emission, measured with a small aperture ($<2''$), is used to estimate the power of AGNs. After the publication of Imanishi (2003), such photometric data have been presented by Gorjian et al. (2004). These photometric measurements for Seyfert 1s in our sample are summarized in column 9 of Table 1. The same data for Seyfert 2s, studied by Imanishi (2003), together with the estimated nuclear 3.3 μm PAH emission luminosities, are summarized in Table 7. Figure 3d compares the nuclear N -band luminosity measured with a 1.⁵ aperture (Gorjian et al. 2004) and nuclear 3.3 μm PAH emission luminosities in Seyfert 1s and 2s. As were the cases for Figs. 3a, 3b, and 3c, we see no clear evidence that Seyfert 2s are distributed at substantially upper-left locations, as compared to Seyfert 1s.

The ring-shaped kpc-scale circumnuclear starbursts correspond to 1.5–7 arcsec for the observed Seyfert galaxies at $z=0.008$ –0.035. Thus, if circumnuclear starbursts are important, the N -band photometry measured with $>4''$ apertures should be systematically higher than that with the 1.⁵ aperture. For the majority of the Seyfert 1s in Table 1, both measurements are available, but they indicate that this is not the case. In fact, although the circumnuclear starbursts were clearly detected in the two nearby well-studied Seyferts, NGC 1068 and NGC 7469 (Miles et al. 1996; Le Floc'h et al. 2001), they were not commonly found in the N -band images of the majority of Seyferts (Gorjian et al. 2004). It is likely that possible time variation of the nuclear N -band emission (Gorjian et al. 2004), rather than the inclusion or exclusion of the circumnuclear starbursts, has more severe effects for the comparison of the nuclear 3.3 μm PAH emission luminosities and ground-based N -band luminosity measurements. In this regard, the absence of a significant distribution change of Seyfert 2s from Fig. 3c to Fig. 3d is reasonable.

Another powerful indicator of the power of AGNs is radio emission. Radio emission from the core of a Seyfert galaxy can be taken as AGN emission and suffers virtually no effects of extinction by the dusty torus. Core radio emission data, measured with 0.²⁵ spatial

resolution, are available for many of the CfA and 12 μm Seyferts (Kukula et al. 1995; Thean et al. 2000). These core radio data for Seyfert 1s and 2s are summarized in Table 1 (column 10) and Table 7 (column 5), respectively. Figure 3e plots the comparison between the core radio luminosities at 8.4 GHz and nuclear 3.3 μm PAH emission luminosities in both Seyfert 1s and 2s. Again, in this plot, we see no clear trend that Seyfert 2s are distributed to the upper-left side of Seyfert 1s.

The 2–10 keV X-ray luminosity can also provide a good indication of the power of an AGN, because an AGN usually produces 2–10 keV emission far more strongly than does star-formation. Some fraction of the Seyfert 1s and 2s in our sample have available 2–10 keV X-ray observations (Turner et al. 1997; George et al. 1982). However, unlike previous AGN-power indicators where *observed* luminosities have been used, *absorption-corrected* luminosity is essential for 2–10 keV emission, particularly for Seyfert 2s. This absorption-correction can be uncertain for many Seyfert 2s, because as many as half of all Seyfert 2s are Compton thick ($N_{\text{H}} > 10^{24} \text{ cm}^{-2}$; Risaliti et al. 1999), in which case, observed 2–10 keV emission is dominated by a reflected/scattered component, rather than by a direct transmitted component, making estimates of the absorption-corrected 2–10 keV luminosities highly uncertain. For Seyfert 1s, the absorption correction was thought to be more straightforward and often insignificant, but recent X-ray data of the Seyfert 1 galaxy, Mrk 231, imply that the correction can be more complicated than has been anticipated (Braito et al. 2004). Additionally, the fraction of Seyferts in our sample with available absorption-corrected 2–10 keV X-ray luminosities is smaller than that with other previous AGN-power indicators. No comparison between the 2–10 keV X-ray and nuclear 3.3 μm PAH emission luminosities is made in this paper.

To summarize the above comparisons between the luminosities of the nuclear starbursts and AGNs in Figs. 3a–3e, Seyfert 1s and 2s have nuclear starbursts of similar strength, with respect to the AGN luminosities. We see no clear evidence that Seyfert 2s have systematically more powerful nuclear starbursts than do Seyfert 1s.

In Seyfert 2s, the correlation between nuclear 3.3 μm PAH emission luminosities and *IRAS* 12 μm , *IRAS* 25 μm , and ground-based *N*-band (10.6 μm) luminosities measured with $>4''$ apertures, was statistically confirmed (Imanishi 2003), which suggests that the powers of nuclear starbursts and AGNs are correlated. We apply the generalized Kendall’s rank correlation statistic (Isobe, Feigelson, & Nelson 1986)² to both types of Seyferts in Figs 3a–3e. The probability that a correlation is not present is found to be 0.01%, <0.01%, 0.05%, 0.8%, and 0.6% for Fig. 3a, 3b, 3c, 3d, and 3e, respectively. Thus, the correlation between

²software is available at: <http://www.astro.psu.edu/statcodes/>.

the luminosities of the nuclear starbursts in the dusty tori and central AGNs is statistically confirmed in Seyfert galaxies in all the plots in Fig. 3, suggesting the nuclear starburst-AGN connection. The enhancement of a mass accretion rate onto a central supermassive black hole, owing to the increased turbulence of molecular gas in the torus because of the presence of nuclear starbursts (Wada & Norman 2002), is one possible scenario that could account for the luminosity correlation.

Figures 4a and 4b show, respectively, the histograms of the redshifts and infrared luminosities of the observed Seyfert 1s and 2s. Although the fraction of high redshift sources is slightly higher in Seyfert 1s than 2s, the distribution of the infrared luminosities is similar. Thus, the above conclusions cannot be caused by the different luminosity distribution between the Seyfert 1 and 2 samples. If Seyfert galaxies at higher redshifts had stronger nuclear starbursts, relative to the AGN power, than those at lower redshifts, our conclusions could be affected by some bias caused by the slightly different redshift distribution between Seyfert 1s and 2s. However, the redshift range probed by our study is only 0.008–0.035, where no strong cosmological evolution is expected, and so this scenario seems very unlikely.

Figures 5a and 5b show, respectively, the rest-frame equivalent widths of the $3.3\text{ }\mu\text{m}$ PAH emission feature ($\text{EW}_{3.3\text{PAH}}$) and the observed spectroscopic CO indices (CO_{spec}) of the Seyfert 1s and 2s. Both the $\text{EW}_{3.3\text{PAH}}$ and CO_{spec} values are systematically smaller in Seyfert 1s than in Seyfert 2s. This trend is reasonably explained by the higher contributions from the featureless AGN continuum to the near-infrared fluxes in Seyfert 1s, owing to less attenuation, which decrease both the $\text{EW}_{3.3\text{PAH}}$ and CO_{spec} values, as compared to Seyfert 2s.

The overall results revealed through the present datasets favor the *slightly-modified* AGN unification theory, in which: (1) the central engines of both Seyfert 1s and 2s are intrinsically the same, but those of Seyfert 2s are obscured by dusty tori; (2) the dusty tori not only obscure and re-radiate AGN light as infrared dust emission, but also *contain nuclear starbursts in both Seyfert 1s and 2s of similar strength*; and (3) *the nuclear starbursts have close physical connections to the central AGNs*.

The presence of the nuclear starbursts in the dusty torus has some important implications for AGN research. First, in the calculation of infrared dust emission from the torus, only radiation from the central AGN has usually been taken into account as a heating energy source. Although the absolute magnitudes of the nuclear starbursts, estimated in this paper and by Imanishi (2003), are not very powerful, in terms of the infrared luminosity from a whole Seyfert galaxy, the inclusion of nuclear starbursts may help us to better understand emission from the dusty torus of a Seyfert galaxy (van Bemmel & Dullemond 2003). Next, theoretically, the nuclear starbursts can naturally occur in an extended (tens pc) torus, but

they are difficult to produce in a compact (smaller than a few pc) torus (Wada & Norman 2002; Wada et al. in preparation). Our detection of nuclear starbursts may suggest that the extended torus model is more plausible in Seyfert galaxies. Finally, radiation from nuclear starbursts could affect the mass accretion rate onto a central supermassive black hole (Umemura, Fukue, & Mineshige 1998; Ohsuga et al. 1999). So far, more powerful, but more distant, *circumnuclear* starbursts have been considered as the primary radiation source (Umemura, Fukue, & Mineshige 1997), but *nuclear* starbursts, even though less powerful, may have important effects in this respect, because of their proximity to the central supermassive black hole.

5.3. Do the CfA and 12 μm Seyfert 1 Galaxies Have Different Nuclear Star Formation Properties?

So far we have combined the CfA and 12 μm Seyfert 1s, and conducted a comparison with Seyfert 2s in the same samples. It is of interest to compare nuclear star formation properties, by dividing Seyfert 1s into two separate samples, as was done for Seyfert 2s by Imanishi & Alonso-Herrero (2004). Figure 6 plots the distribution of CO_{spec} , $\text{EW}_{3.3\text{PAH}}$, and $\text{L}_{\text{nuclear-3.3PAH}}/\text{L}_{\text{IR}}$, by separating the Seyfert 1s into two samples. In all the plots, no systematic differences can be seen between Seyfert 1s in the CfA and 12 μm samples.

Imanishi & Alonso-Herrero (2004) previously found no systematic difference in Seyfert 2s between CfA and 12 μm samples. When combined with the absence of a difference in Seyfert 1s, we can argue that the nuclear star formation properties of both Seyfert 1s and 2s in the CfA sample are similar to those in the 12 μm sample. In particular, the $\text{L}_{\text{nuclear-3.3PAH}}/\text{L}_{\text{IR}}$ ratios in Fig. 6c trace the relative contribution from nuclear starbursts to the infrared luminosity. Ho & Ulvestad (2001) put forward the possibility that 12 μm Seyferts may be biased to those with unusually elevated levels of nuclear star formation, because nuclear star formation can be a strong 12 μm emitter. However, our studies provide no support for this.

6. Summary

We presented near-infrared K - and L -band spectroscopic results of 23 Seyfert 1 galaxies in CfA and 12 μm samples. Our L -band spectroscopic method successfully detected 3.3 μm PAH emission, the signature of nuclear star formation, in a significant fraction ($=43\%$) of the observed Seyfert 1 nuclei. The high surface brightness values of the 3.3 μm PAH

emission suggested that the detected signatures are most likely to come from putative nuclear starbursts in the dusty tori, rather than from quiescent star-formation in the nuclear regions of these Seyfert 1 galaxies. The properties of the nuclear starbursts in Seyfert 1s were compared with those in Seyfert 2s; we found that Seyfert 1s possess nuclear starbursts with similar luminosities to those of Seyfert 2s. The nuclear starburst luminosities positively correlated with the AGN luminosities in a statistical sense, suggesting nuclear starburst-AGN connections in both Seyfert 1s and 2s. No systematic differences in the nuclear star formation properties were found between Seyfert 1s in the CfA and 12 μm samples, as previously found in Seyfert 2s; this suggested that 12 μm Seyferts are not strongly biased to those with enhanced nuclear star formation activity, as compared to the CfA sample.

We are grateful to P. Sears, S. B. Bus (IRTF) and H. Terada, and R. Potter (Subaru) for their supports during our observing runs. The referee, D. Sanders, gave useful comments on the manuscript. KW is supported by Grant-in-Aids for Scientific Research (no. 15684003). Some part of the data analysis was made using a computer system operated by the Astronomical Data Analysis Center (ADAC) and the Subaru Telescope of the National Astronomical Observatory, Japan. This research has made use of the SIMBAD database, operated at CDS, Strasbourg, France, and of the NASA/IPAC Extragalactic Database (NED) which is operated by the Jet Propulsion Laboratory, California Institute of Technology, under contract with the National Aeronautics and Space Administration.

REFERENCES

Alonso-Herrero, A., Ivanov, V. D., Jayawardhana, R., & Hosokawa, T. 2002, *ApJ*, 571, L1

Alonso-Herrero, A., Quillen, A. C., Rieke, G. H., Ivanov, V., & Efstathiou, A. 2003, *AJ*, 126, 81

Alonso-Herrero, A., Simpson, C., Ward, M. J., & Wilson, A. S. 1998, *ApJ*, 495, 196

Antonucci, R. 1993, *ARA&A*, 31, 473

Braito, V. et al. 2004, *A&A*, 420, 79

Coziol, R., Doyon, R., & Demers, S. 2001, *MNRAS*, 325, 1081

Doyon, R., Joseph, R. D., & Wright, G. S. 1994, *ApJ*, 421, 101

Fabian, A. C., Barcons, X., Almaini, O., & Iwasawa, K. 1998, *MNRAS*, 297, L11

George, I. M., Turner, T. J., Netzer, H., Nandra, K., Mushotzky, R. F., & Yaqoob, T. 1998, *ApJS*, 114, 73

Glass, I. S., Moorwood, A. F. M., & Eichendorf, W. 1982, *A&A*, 107, 276

Gonzalez Delgado, R. M., Heckman, T., & Leitherer, C. 2001, *ApJ*, 546, 845

Gorjian, V., Werner, M. W., Jarrett, T. H., Cole, D. M., & Ressler, M. E. 2004, *ApJ*, 605, 156

Heckman, T. M. 2001, in *ASP Conf. Ser.* 240, *Gas and Galaxy Evolution*, ed. J. E. Hibbard, M. Rupen, & J. H. van Gorkom (San Francisco: ASP), 345 (astro-ph/0009075)

Heckman, T. M., Gonzalez Delgado, R., Leitherer, C., Meurer, G. R., Krolik, J., Wilson, A. S., Koratkar, A., & Kinney, A. 1997, *ApJ*, 482, 114

Ho, L. C., & Ulvestad, J. S. 2001, *ApJS*, 133, 77

Huchra, J., & Burg, R. 1992, *ApJ*, 393, 90

Imanishi, M. 2002, *ApJ*, 569, 44

Imanishi, M. 2003, *ApJ*, 599, 918

Imanishi, M., & Alonso-Herrero, A. 2004, *ApJ*, 614, in press (astro-ph/0407215)

Imanishi, M., & Dudley, C. C. 2000, *ApJ*, 545, 701

Isobe, T., Feigelson, E. D., & Nelson, P. I. 1986, *ApJ*, 306, 490

Ivanov, V. D., Rieke, G. H., Groppi, C. E., Alonso-Herrero, A., Rieke, M. J., & Engelbracht, C. W. 2000, *ApJ*, 545, 190

Kennicutt, R. C. Jr. 1998, *ARA&A*, 36, 189

Kleinmann, D. E., & Low, F. J. 1970, *ApJ*, 161, L203

Kobayashi, N., et al. 2000, *Proc. SPIE*, 4008, 1056

Kukula, M. J., Pedlar, A., Baum, S. A., & O'Dea, C. P. 1995, *MNRAS*, 276, 1262

Le Floc'h, E., Mirabel, I. F., Laurent, O., Charmandaris, V., Gallais, P., Sauvage, M., Vigroux, L., & Cesarsky, C. 2001, *A&A*, 367, 487

Levenson, N. A., Krolik, J. H., Zycki, P. T., Heckman, T. M., Weaver, K. A., Awaki, H., & Terashima, Y. 2002, *ApJ*, 573, L81

Maiolino, R., Ruiz, M., Rieke, G. H., & Keller, L. D. 1995, *ApJ*, 446, 561

Marco, O., & Alloin, D. 1998, *A&A*, 336, 823

Miles, J. W., Houck, J. R., Hayward, T. L., & Ashby, M. L. N. 1996, *ApJ*, 465, 191

Mouri, H., Kawara, K., Taniguchi, Y., & Nishida, M. 1990, *ApJ*, 356, L39

Ohsuga, K., Umemura, M., Fukue, J., & Mineshige, S. 1999, *PASJ*, 51, 345

Oliva, E., Origlia, L., Maiolino, R., & Moorwood, A. F. M. 1999, *A&A*, 350, 9

Perez Garcia, A. M., & Rogriguez Espinosa, J. M. 2001, *ApJ*, 557, 39

Pier, E. A. & Krolik, J. H. 1992, *ApJ*, 401, 99

Rayner, J. T., Toomey, D. W., Onaka, P. M., Denault, A. J., Stahlberger, W. E., Vacca, W. D., Cushing, M. C., & Wang, S. 2003, *PASP*, 115, 362

Rieke, G. H. 1978, *ApJ*, 226, 550

Rieke, G. H., & Lebofsky, M. J. 1985, *ApJ*, 288, 618

Risaliti, G., Maiolino, R., & Salvati, M. 1999, *ApJ*, 522, 157

Rodriguez-Ardila, A., & Viegas, S. M. 2003, *MNRAS*, 340, L33

Rodriguez Espinosa, J. M., & Perez Garcia, A. M. 1997, *ApJ*, 487, L33

Rush, B., Malkan, M. A., & Spinoglio, L. 1993, *ApJS*, 89, 1

Sanders, D. B., & Mirabel, I. F. 1996, *ARA&A*, 34, 749

Seyfert, C. K. 1943, *ApJ*, 97, 28

Spinoglio, L., & Malkan, M. A. 1989, *ApJ*, 342, 83

Storchi-Bergmann, T., Wilson, A. S., & Baldwin, J. A. 1996, *ApJ*, 460, 252

Thean, A., Pedlar, A., Kukula, M. J., Baum, S. A., & O'Dea, C. P. 2000, *MNRAS*, 314, 573

Tokunaga, A. T. 2000, in *Allen's Astrophysical Quantities*, ed. A. N. Cox (4th ed; Berlin: Springer), 143

Turner, T. J., George, I. M., Nandra, K., & Mushotzky, R. F. 1997, *ApJS*, 113, 23

Umemura, M., Fukue, J., & Mineshige, S. 1997, *ApJ*, 479, L97

Umemura, M., Fukue, J., & Mineshige, S. 1998, *MNRAS*, 299, 1123

van Bemmel, I. M., & Dullemond, C. P. 2003, *A&A*, 404, 1

Wada, K., & Norman, C. A. 2002, *ApJ*, 566, L21

Willner, S. P., Ward, M., Longmore, A., Lawrence, A., Fabbiano, G., & Elvis, M., 1984, *PASP*, 96, 143

Table 1. Detailed Information on the Observed Seyfert 1 Galaxies

Object (1)	Redshift (2)	f_{12} (Jy) (3)	f_{25} (Jy) (4)	f_{60} (Jy) (5)	f_{100} (Jy) (6)	$\log L_{\text{IR}}$ (ergs s $^{-1}$) (7)	f_N (Jy) (8)	$f_N(1'5)$ (Jy) (9)	$\log f_{8.4\text{GHz}}$ (mJy beam $^{-1}$) (10)	Remarks (11)
Mrk 335	0.025	0.30	0.38	0.34	<0.57	44.2 (10.6)	0.21 (i)	0.15	1.89	CfA, 12 μ m
NGC 863 (Mrk 590)	0.027	0.19	0.22	0.49	1.46	44.2 (10.6)	0.15 (ii)	...	3.44	CfA
NGC 3786 (Mrk 744)	0.009	0.10 ^a	0.39 ^a	1.20 ^a	3.00 ^a	43.4 (9.8)	0.059 (ii)	...	0.86	CfA
NGC 4235	0.008	<0.13	<0.16	0.32	0.65	42.5–43.0 (8.9–9.4)	0.034 (ii)	...	5.22	CfA
NGC 4253 (Mrk 766) ^b	0.013	0.39	1.30	4.03	4.66	44.2 (10.6)	0.24 (ii)	0.25	4.77	CfA, 12 μ m
NGC 5548	0.017	0.40	0.77	1.07	1.61	44.2 (10.6)	0.20 (iii)	0.29	2.07	CfA, 12 μ m
Mrk 817	0.031	0.34	1.18	2.12	2.27	44.8 (11.2)	...	0.23	3.45	CfA, 12 μ m
NGC 5940	0.034	<0.17	0.11	0.74	1.75	44.3–44.4 (10.7–10.8)	0.026 (ii)	CfA
2237+07 (UGC 1238)	0.025	0.20	0.34	0.83	<2.49	44.2–44.3 (10.6–10.7)	0.063 (ii)	...	1.73	CfA
NGC 7469	0.016	1.35	5.79	25.87	34.90	45.1 (11.5)	0.60 (i)	0.31	13.63	CfA, 12 μ m
Mrk 530 (NGC 7603)	0.029	0.16	<0.25	0.85	2.04	44.3–44.4 (10.7–10.8)	0.077 (i)	0.10	2.78	CfA, 12 μ m
NGC 931 (Mrk 1040)	0.016	0.61	1.32	2.56	4.55	44.4 (10.8)	0.33 (ii)	0.21	...	12 μ m
F03450+0055	0.031	0.28	0.51	0.47	<3.24	44.4–44.6 (10.8–11.0)	0.17 (ii)	0.10	4.2	12 μ m
3C 120	0.033	0.29	0.64	1.28	2.79	44.7 (11.1)	0.22 (i)	0.11	...	12 μ m
Mrk 618	0.035	0.34	0.79	2.71	4.24	44.9 (11.3)	0.27 (ii)	<0.06	1.7	12 μ m
MCG-5-13-17	0.013	0.22	0.57	1.40	1.99	43.8 (10.2)	...	0.14	1.4	12 μ m
Mrk 79	0.022	0.31	0.76	1.50	2.36	44.4 (10.8)	0.26 (ii)	0.24	0.8	12 μ m
NGC 2639	0.011	0.16	0.21	1.99	7.06	43.8 (10.2)	0.008 (ii)	<0.14	90.6	12 μ m
Mrk 704	0.030	0.35	0.53	0.36	<0.77	44.4–44.5 (10.8–10.9)	0.27 (ii)	0.30	0.7	12 μ m
NGC 2992	0.008	0.59	1.37	6.87	14.4	44.0 (10.4)	0.20 (iv)	0.16	3.9	12 μ m
Mrk 1239 ^b	0.019	0.65	1.14	1.34	<2.42	44.4 (10.8)	0.60 (ii)	0.29	6.8	12 μ m
UGC 7064	0.025	0.17	0.38	2.75	5.57	44.6 (11.0)	12 μ m
MCG-2-33-34	0.014	0.17	0.37	1.16	2.22	43.8 (10.2)	...	<0.03	0.6	12 μ m
IC 4329A	0.016	1.08	2.21	2.03	1.66	44.5 (10.9)	0.77 (i)	0.92	4.9	12 μ m
Mrk 509	0.035	0.32	0.70	1.36	1.52	44.8 (11.2)	0.24 (ii)	0.20	1.8	12 μ m

Note. — Column (1): Object. CfA Seyfert 1s are placed first. Ordered by right ascension in each Seyfert 1 sample. Column (2): Redshift. Columns (3)–(6): f_{12} , f_{25} , f_{60} , and f_{100} are *IRAS FSC* fluxes at 12 μ m, 25 μ m, 60 μ m, and 100 μ m, respectively. Column (7): Logarithm of infrared (8–1000 μ m) luminosity in ergs s $^{-1}$ calculated with $L_{\text{IR}} = 2.1 \times 10^{39} \times D(\text{Mpc})^2 \times (13.48 \times f_{12} + 5.16 \times f_{25} + 2.58 \times f_{60} + f_{100})$ ergs s $^{-1}$ (Sanders & Mirabel 1996). The values in parenthesis are logarithm of infrared luminosities in units of solar luminosities. Column (8): Ground-based N -band (10.6 μ m) photometric measurement using a single element detector ($>4''$ aperture) and references. (i): Rieke 1978; (ii): Maiolino et al. 1995; (iii) Kleinmann & Low 1970; (iv) Glass, Moorwood, & Eichendorf 1982. Column (9): Ground-based N -band (10.6 μ m) photometry measured using a two-dimensional camera with a 1''5

aperture (Gorjian et al. 2004). Column (10): Peak radio intensity at 8.4 GHz, measured with 0''.25 resolution radio images (Kukula et al. 1995; Thean et al. 2000). Column (11): CfA (Huchra & Burg 1992) or 12 μ m (Rush et al. 1993) Seyfert 1.

^aISO measurements (Perez Garcia & Rodriguez Espinosa 2001). The f_{12} and f_{100} are extrapolated and interpolated, respectively, from measurements at other wavelengths.

^bObserved by Rodriguez-Ardila & Viegas (2003).

Table 2. Observing Log

Object (1)	Date (UT) (2)	Telescope & Instrument (3)	Integration Time (min) (4)	Standard Star				
				Star Name (5)	L-mag (6)	K-mag (7)	Type (8)	T _{eff} (K) (9)
Mrk 335	2003 Sep 6	IRTF SpeX	40	HR 217	5.1	5.2	F8V	6000
NGC 863	2003 Sep 7	IRTF SpeX	60	HR 650	4.1	4.2	F8V	6000
NGC 3786	2003 Mar 19	IRTF SpeX	30	HR 4412	5.0	5.0	F7V	6240
NGC 4235	2003 Mar 21	IRTF SpeX	20	HR 4708	5.0	5.0	F8V	6000
NGC 5548	2003 Mar 21	IRTF SpeX	20	HR 5423	4.7	4.8	G5V	5700
Mrk 817	2003 Mar 21	IRTF SpeX	20	HR 5581	4.3	4.3	F7V	6240
NGC 5940	2003 Mar 21	IRTF SpeX	20	HR 5659	5.1	5.1	G5V	5700
2237+07	2003 Sep 6	IRTF SpeX	40	HR 8514	4.9	5.0	F6V	6400
NGC 7469	2002 Aug 19	Subaru IRCS	10	HR 8653	4.7	...	G8IV	5400
Mrk 530	2003 Sep 6	IRTF SpeX	40	HR 8772	5.3	5.3	F8V	6000
NGC 931	2003 Sep 6	IRTF SpeX	40	HR 720	4.4	4.5	G0V	5930
F03450+0055	2003 Sep 6	IRTF SpeX	40	HR 962 ^a	3.7	3.7	F8V	6000
3C 120	2003 Sep 7	IRTF SpeX	56	HR 1232 ^b	3.9	4.0	G9V	5400
Mrk 618	2003 Sep 6	IRTF SpeX	60	HR 1232 ^a	3.9	4.0	G9V	5400
MCG-5-13-17	2003 Sep 7	IRTF SpeX	40	HR 1785	5.2	5.3	F6V	6400
Mrk 79	2003 Mar 18	IRTF SpeX	30	HR 3028	4.8	4.8	F6V	6400
NGC 2639	2003 Mar 21	IRTF SpeX	40	HR 3309	4.7	4.7	G5V	5700
Mrk 704	2003 Mar 19	IRTF SpeX	30	HR 3650	4.6	4.6	G9V	5400
NGC 2992	2003 Mar 19	IRTF SpeX	30	HR 3901	5.0	5.1	F8V	6000
UGC 7064	2003 Mar 21	IRTF SpeX	30	HR 4550	4.6	4.6	G8V	5400
MCG-2-33-34	2003 Mar 21	IRTF SpeX	20	HR 4856	4.9	4.9	F7V	6240
IC 4329A	2003 Mar 20	IRTF SpeX	12	HR 5212 ^c	4.8	4.8	F7V	6240
Mrk 509	2003 Sep 6	IRTF SpeX	40	HR 7715 ^d	4.5	4.5	F7V	6240

Note. — Column (1): Object. Column (2): Observing date in UT. Column (3): Instrument used for spectroscopy. Column (4): Net on-source integration time in min. Column (5): Standard star name. Column (6): Adopted *L*-band magnitude. Column (7): Adopted *K*-band magnitude. Column (8): Stellar spectral type. Column (9): Effective temperature.

^aHR 720 is used as a standard star for the *K*-band spectrum, because signals of HR 962 in the *K*-band are above the linearity level of the SpeX array.

^bHR 1785 is used as a standard star for the *K*-band spectrum.

^cFlux calibration was made using HR 4412.

^dHR 8772 is used as a standard star for the *K*-band spectrum.

Table 3. Properties of the Nuclear 3.3 μ m PAH Emission Feature

Object (1)	$f_{\text{nuclear-3.3PAH}}$ ($\times 10^{-14}$ ergs s^{-1} cm^{-2}) (2)	$L_{\text{nuclear-3.3PAH}}$ ($\times 10^{39}$ ergs s^{-1}) (3)	rest EW _{3.3PAH} (nm) (4)	$L_{\text{nuclear-3.3PAH}}/\text{LIR}$ ($\times 10^{-3}$) (5)	$S_{\text{nuclear-3.3PAH}}$ ($\times 10^{39}$ ergs s^{-1} kpc^{-2}) (6)
Mrk 335	2.5	31	1.4	0.19	36
NGC 863	<2.3	<33	<5.4	<0.20	<33
NGC 3786	<6.4	<10	<7.0	<0.38	<91
NGC 4235	3.4	4.4	8.7	0.5–1.3	49
NGC 4253	6.5 ^a	20.7 ^a	40 ^a	0.14 ^a	230
NGC 5548	<4.3	<25	<4.3	<0.18	<61
Mrk 817	5.4	100	4.3	0.16	78
NGC 5940	2.7	63	9.8	0.23–0.35	41
2237+07	4.4	54	9.8	0.27–0.36	64
NGC 7469	<7.0	<35	<2.4	0.026	<390
Mrk 530	4.6	76	1.5	0.33–0.39	67
NGC 931	<4.3	<22	<2.3	<0.091	<61
F03450+0055	<3.8	<73	<2.2	<0.28	<57
3C 120	4.9	110	1.9	0.21	76
Mrk 618	2.9	71	3.1	0.081	44
MCG-5-13-17	<4.8	<16	<9.5	<0.23	<67
Mrk 79	<4.9	<47	<2.6	<0.19	<71
NGC 2639	<1.7	<3.9	<9.5	<0.06	<23
Mrk 704	<2.2	<39	<0.9	<0.15	<32
NGC 2992	<9.1	<12	<2.7	<0.11	<133
Mrk 1239	<1.2 ^a	<8.9 ^a	<2.6 ^a	<0.04 ^a	<47
UGC 7064	<2.4	<30	<9.2	<0.079	<35
MCG-2-33-34	3.8	15	10.3	0.22	54
IC 4329A	<16	<78	<1.3	<0.27	<220
Mrk 509	4.3	100	1.6	0.18	62

Note. — Column (1): Object. Column (2): Observed nuclear 3.3 μ m PAH flux. Column (3): Observed nuclear 3.3 μ m PAH luminosity. Column (4): Rest frame equivalent width of the 3.3 μ m PAH emission. Column (5): Observed nuclear 3.3 μ m PAH to infrared luminosity ratio in units of 10^{-3} , a typical value for starburst galaxies. Column (6): Surface brightness of the nuclear 3.3 μ m PAH emission.

^aTaken from Rodriguez-Ardila & Viegas (2003).

Table 4. Nuclear $K - L$ Color

Object (1)	$K - L$ [mag] (2)
Mrk 335	1.9
NGC 863	0.6
NGC 3786	1.3
NGC 4235	1.1
NGC 5548	1.7
Mrk 817	1.7
NGC 5940	1.3
2237+07	1.2
Mrk 530	1.7
NGC 931	1.7
F03450+0055 ^a	1.8
3C 120 ^a	2.0
Mrk 618 ^a	1.6
MCG-5-13-17	1.0
Mrk 79	1.7
NGC 2639	0.3
Mrk 704	1.7
NGC 2992	1.6
UGC 7064	1.1
MCG-2-33-34	1.1
IC 4329A	2.1
Mrk 509 ^a	1.8

Note. — Column (1): Object.
 Column (2): Nuclear $K - L$ magnitude measured with our slit spectroscopy.

^a K - and L -band magnitudes were measured using different standard stars.

Table 5. $\text{Br}\gamma$ Emission Line

Object (1)	FWHM (km s ⁻¹) (2)	$f_{\text{Br}\gamma}$ ($\times 10^{-14}$ ergs s ⁻¹ cm ⁻²) (3)	$L_{\text{Br}\gamma}$ ($\times 10^{40}$ ergs s ⁻¹) (4)	rest EW $_{\text{Br}\gamma}$ (Å) (5)
Mrk 335	1230	1.9	2.3	9.0
2237+07	2250	0.9	1.1	10.3
Mrk 530	920	0.4	0.7	1.1
NGC 931	2390	2.2	1.1	9.3
F03450	1200	1.8	3.4	8.9
3C 120	4970	4.8	10.4	18.2
Mrk 618	2200	1.4	3.5	10.7
Mrk 79	2590	2.1	2.0	8.5
NGC 2992	2000	4.5	0.6	9.7
MCG-2-33-34	2240	1.9	0.7	25.1
IC 4329A	4660	21.5	10.7	20.2
Mrk 509	3020	5.3	13.0	16.6

Note. — Column (1): Object. Column (2): Full-width at half maximum of the $\text{Br}\gamma$ emission line. Column (3): Observed $\text{Br}\gamma$ emission flux. Column (4): Observed $\text{Br}\gamma$ emission luminosity. Column (5): Rest frame equivalent width of the $\text{Br}\gamma$ emission.

Table 6. CO Absorption Feature

Object (1)	CO _{spec} (2)
NGC 863	0.04
NGC 3786	0.10
NGC 4235	0.08
2237+07	0.05
MCG-5-13-17	0.10
NGC 2639	0.21
UGC 7064	0.10
MCG-2-33-34	0.10

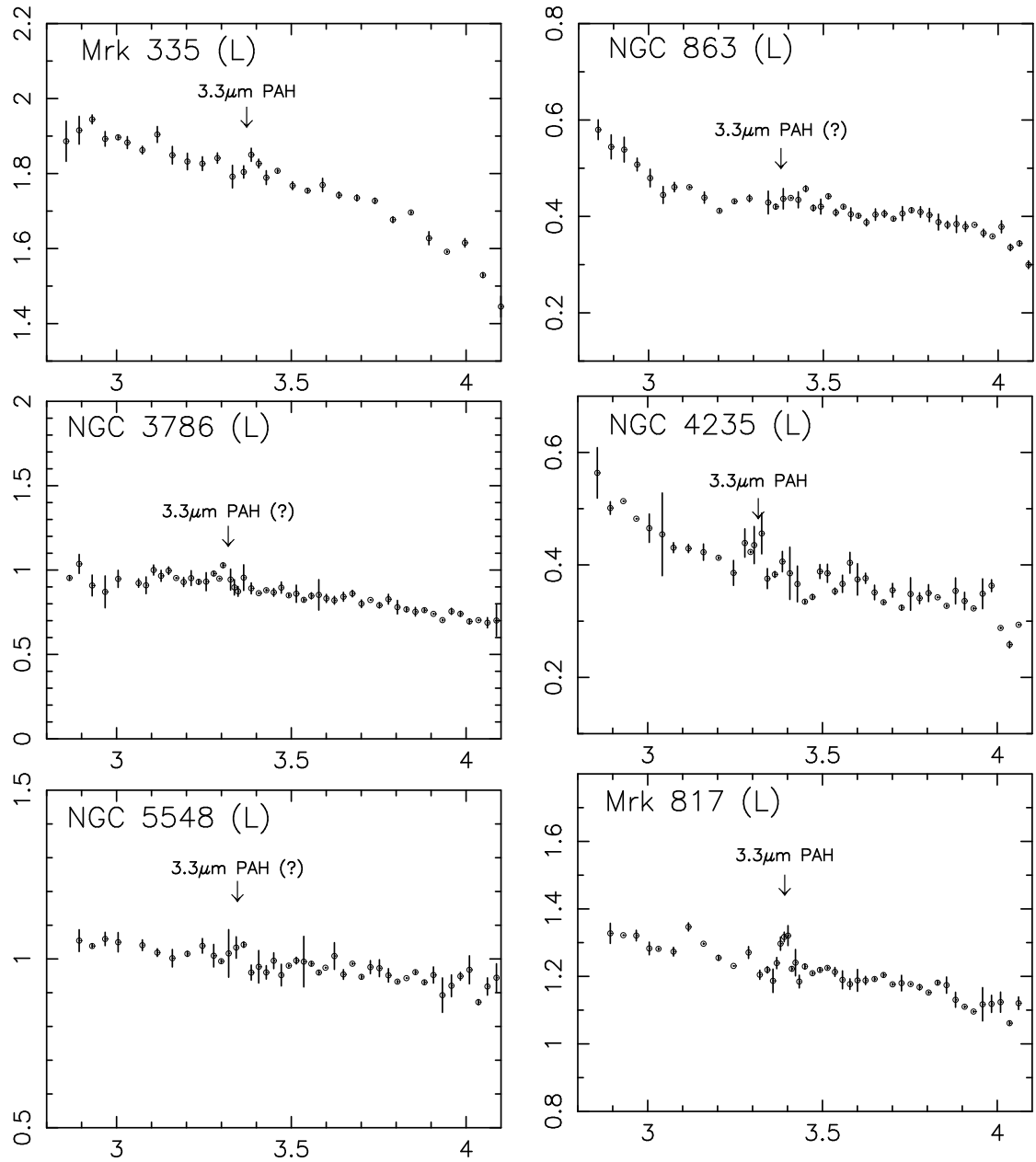
Note. — Column (1): Object. Column (2): Observed spectroscopic CO index.

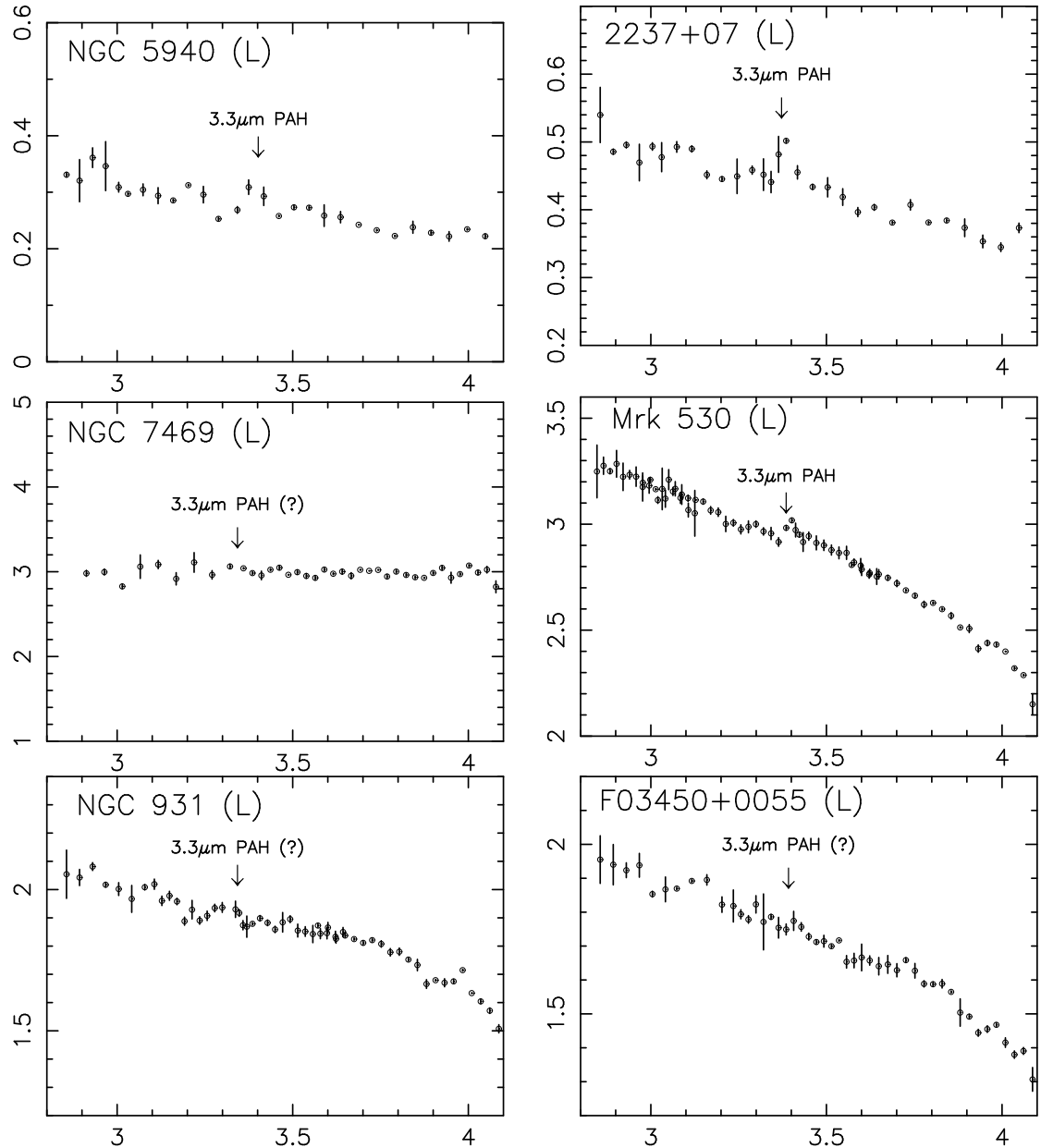
Table 7. Detailed Information on Seyfert 2 Galaxies for Comparison

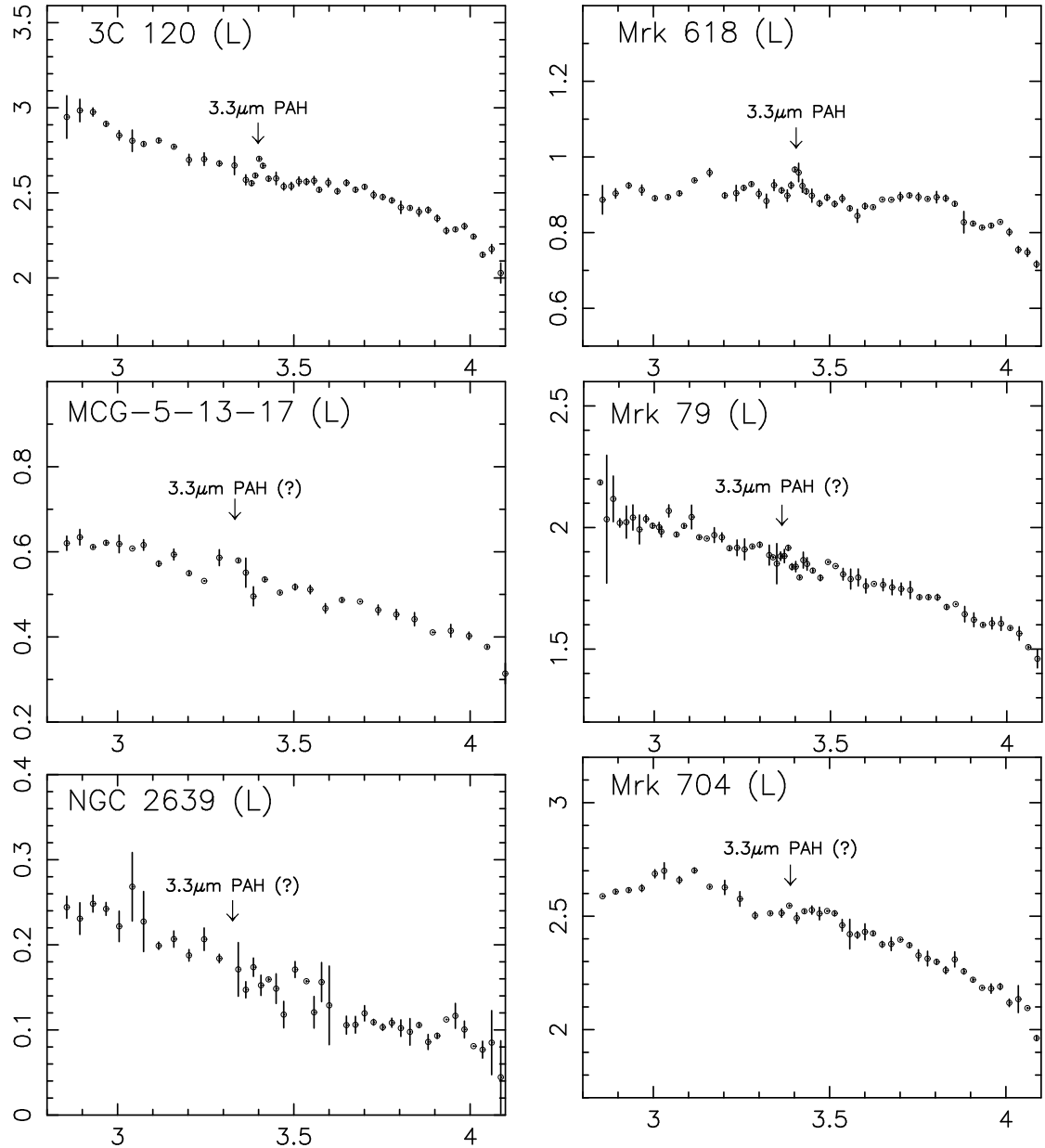
Object (Sy2) (1)	Redshift (2)	$L_{\text{nuclear-3.3PAH}}$ ($\times 10^{39}$ ergs s $^{-1}$) (3)	$f_N(1''.5)$ (Jy) (4)	$f_{8.4\text{GHz}}$ (mJy beam $^{-1}$) (5)	Remarks (6)
Mrk 334	0.022	58	...	1.33	CfA
Mrk 993	0.015	<9.4	...	0.44	CfA
Mrk 573	0.017	<18	...	0.61	CfA
NGC 1144	0.029	<12	...	2.03	CfA, 12 μm
NGC 4388	0.008	<4.7	0.22	2.74	CfA, 12 μm
NGC 5252	0.023	<56	...	4.57	CfA
NGC 5256 (Mrk 266SW)	0.028	133	0.07	3.49	CfA, 12 μm
NGC 5347	0.008	<7.9	0.21	0.7	CfA, 12 μm
NGC 5674	0.025	<19	CfA
NGC 5695	0.014	<6.1	CfA
NGC 5929	0.008	<1.7	<0.03	8.22	CfA, 12 μm
NGC 7674	0.029	136	0.25	...	CfA, 12 μm
NGC 7682	0.017	11	...	12.22	CfA
Mrk 938	0.019	289	0.16	6.2	12 μm
NGC 262 (Mrk 348)	0.015	<38	0.12	310.3	12 μm
NGC 513	0.020	<22	<0.10	0.8	12 μm
F01475-0740	0.017	22	...	132.0	12 μm
NGC 1125	0.011	24	<0.06	4.2	12 μm
NGC 1194	0.013	<8.8	...	0.7	12 μm
NGC 1241	0.014	<4.1	<0.10	5.3	12 μm
NGC 1320 (Mrk 607)	0.010	<12	0.23	0.7	12 μm
F04385-0828	0.015	18	0.16	4.7	12 μm
NGC 1667	0.015	<7.1	<0.10	0.4	12 μm
NGC 3660	0.012	11	<0.11	...	12 μm
NGC 4501	0.008	<4.7	<0.11	...	12 μm , CfA ^a
NGC 4968	0.010	17	0.25	2.8	12 μm
MCG-3-34-64	0.017	<18	0.59	24.5	12 μm
NGC 5135	0.014	58	0.12	...	12 μm
MCG-2-40-4 (NGC 5995)	0.024	<80	0.22	1.6	12 μm
F15480-0344	0.030	<59	0.10	9.5	12 μm
NGC 7172	0.009	<8.4	0.11	2.0	12 μm
MCG-3-58-7	0.032	<78	0.20	0.3	12 μm

Note. — Column (1): Object name of a Seyfert 2 galaxy. Column (2): Redshift. Column (3): Observed nuclear 3.3 μm PAH emission luminosity, taken from Imanishi (2003). Column (4): Observed nuclear N -band flux measured using a two-dimensional camera with a 1''.5 aperture (Gorjian et al. 2004). Column (5): Peak radio intensity at 8.4 GHz measured with 0''.25 spatial resolution (Kukula et al. 1995; Thean et al. 2000). Column (6): CfA or 12 μm Seyfert 2.

^aNGC 4501 is classified as a LINER in the CfA sample (Huchra & Burg 1992).







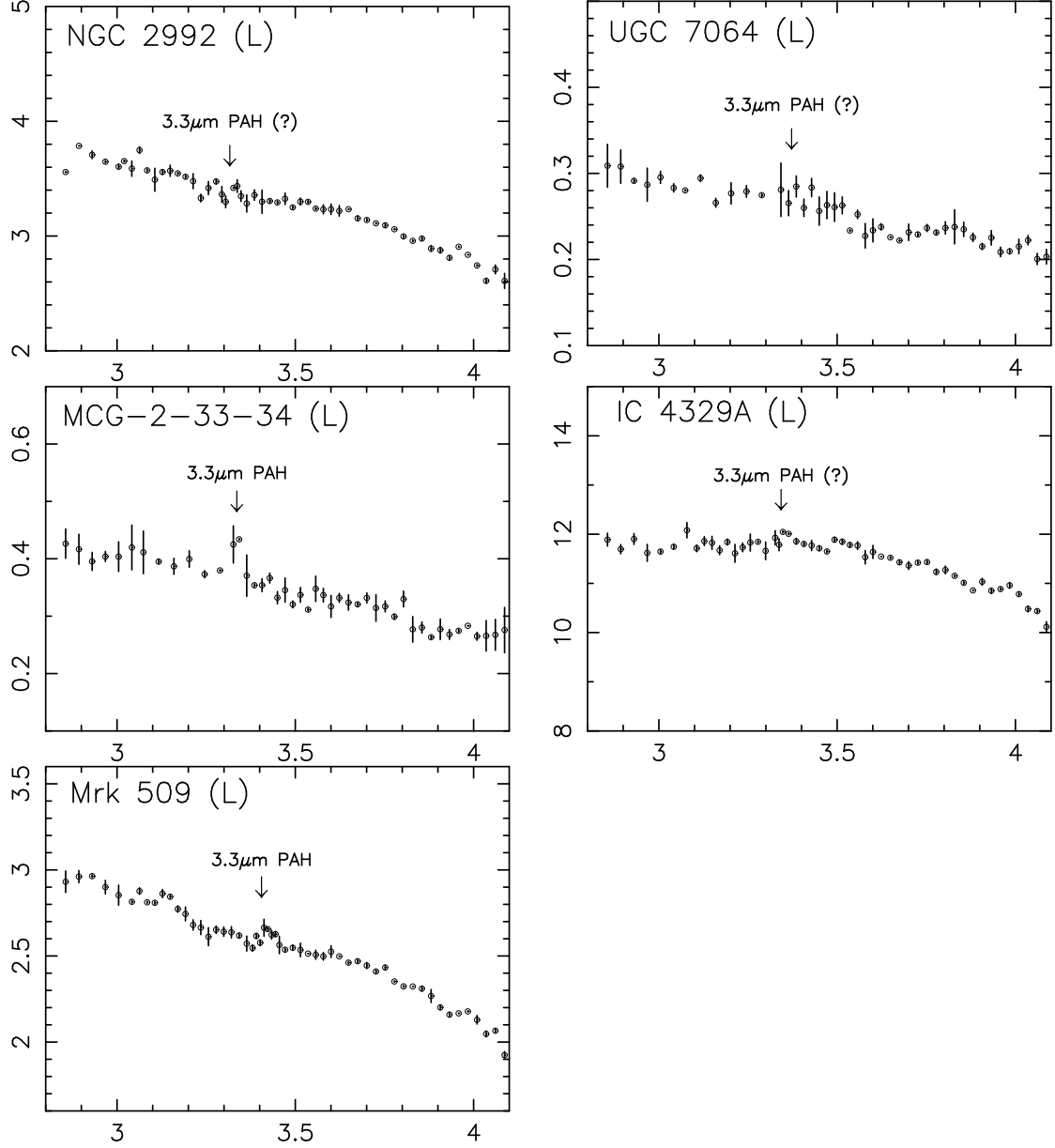
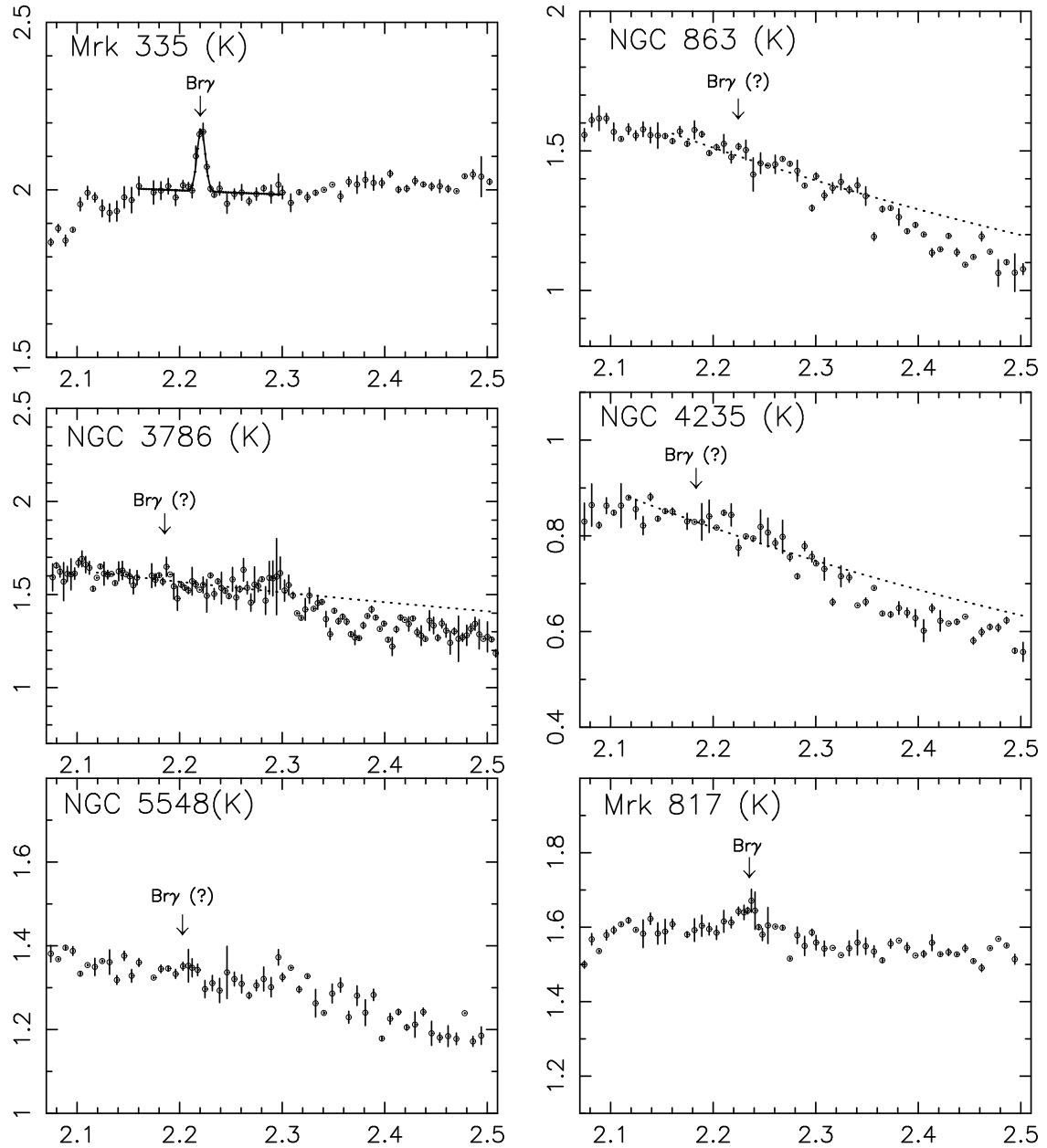
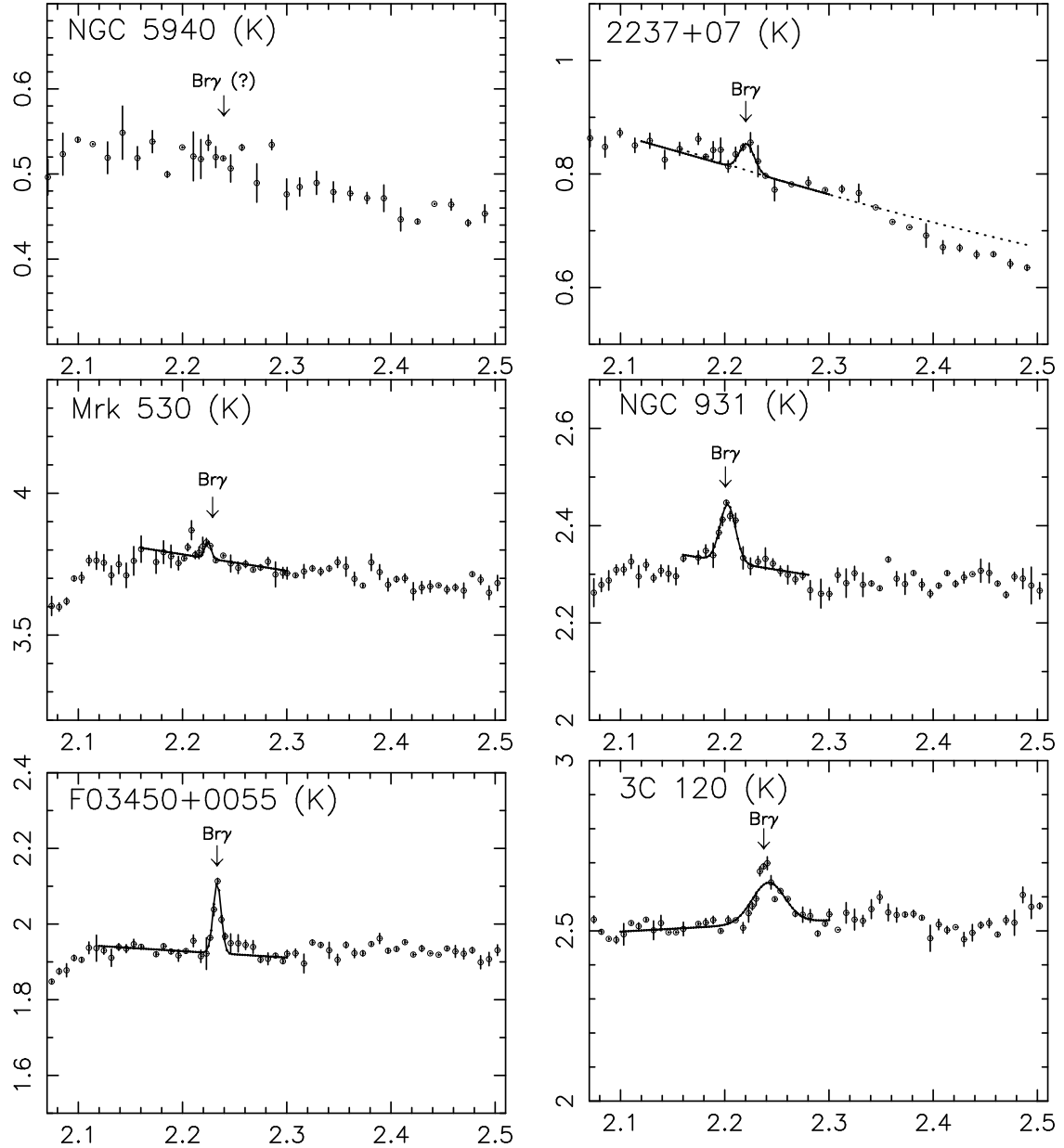
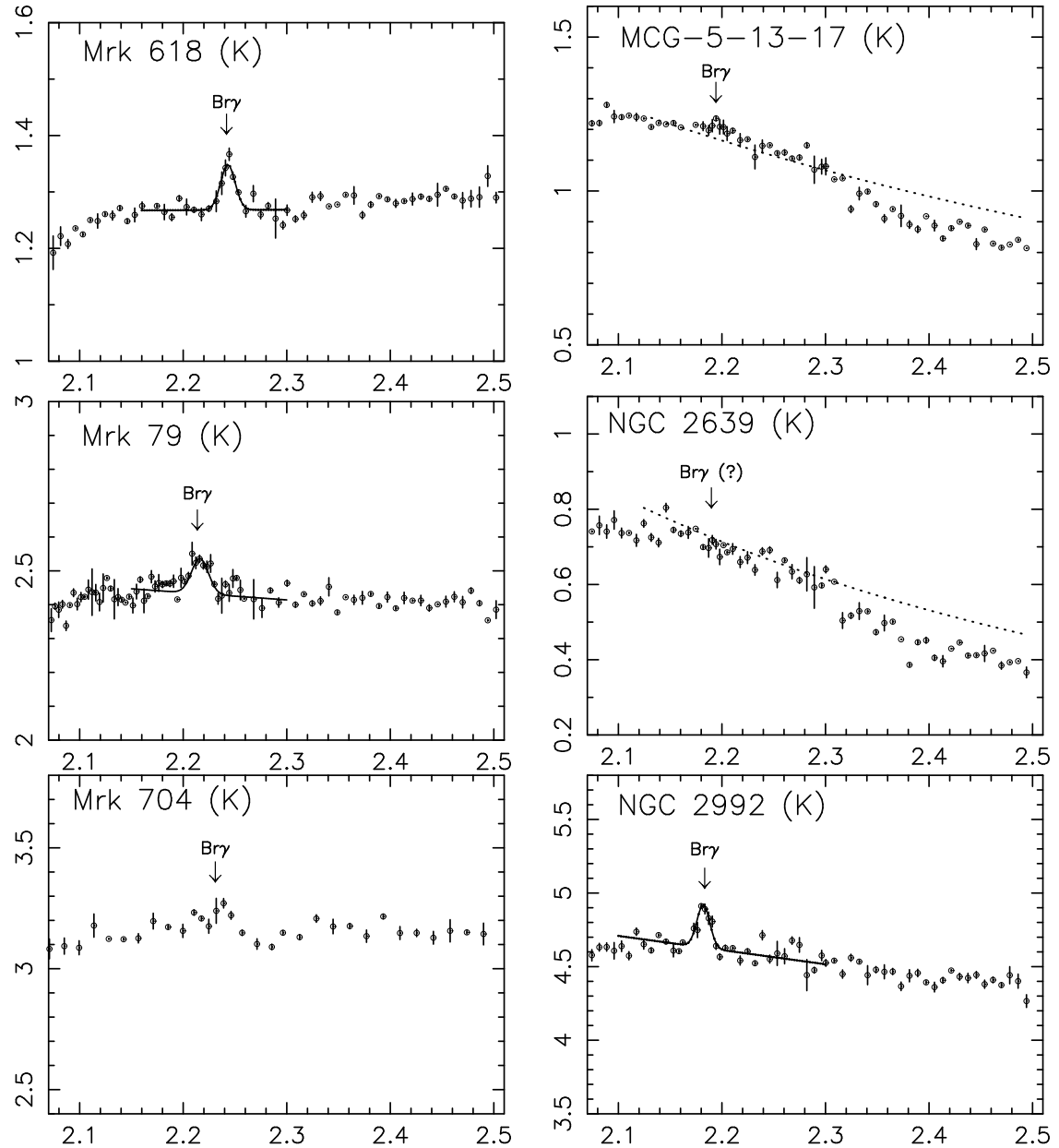


Fig. 1.— Infrared L -band (2.8 – 4.1 μm) slit spectra of the 23 Seyfert 1 nuclei. The abscissa and ordinate are the observed wavelength in μm and F_λ in $10^{-14} \text{ W m}^{-2} \mu\text{m}^{-1}$, respectively. Sources marked with “ $3.3 \mu\text{m}$ PAH” [“ $3.3 \mu\text{m}$ PAH (?)”] show detectable [undetectable] $3.3 \mu\text{m}$ PAH emission features.







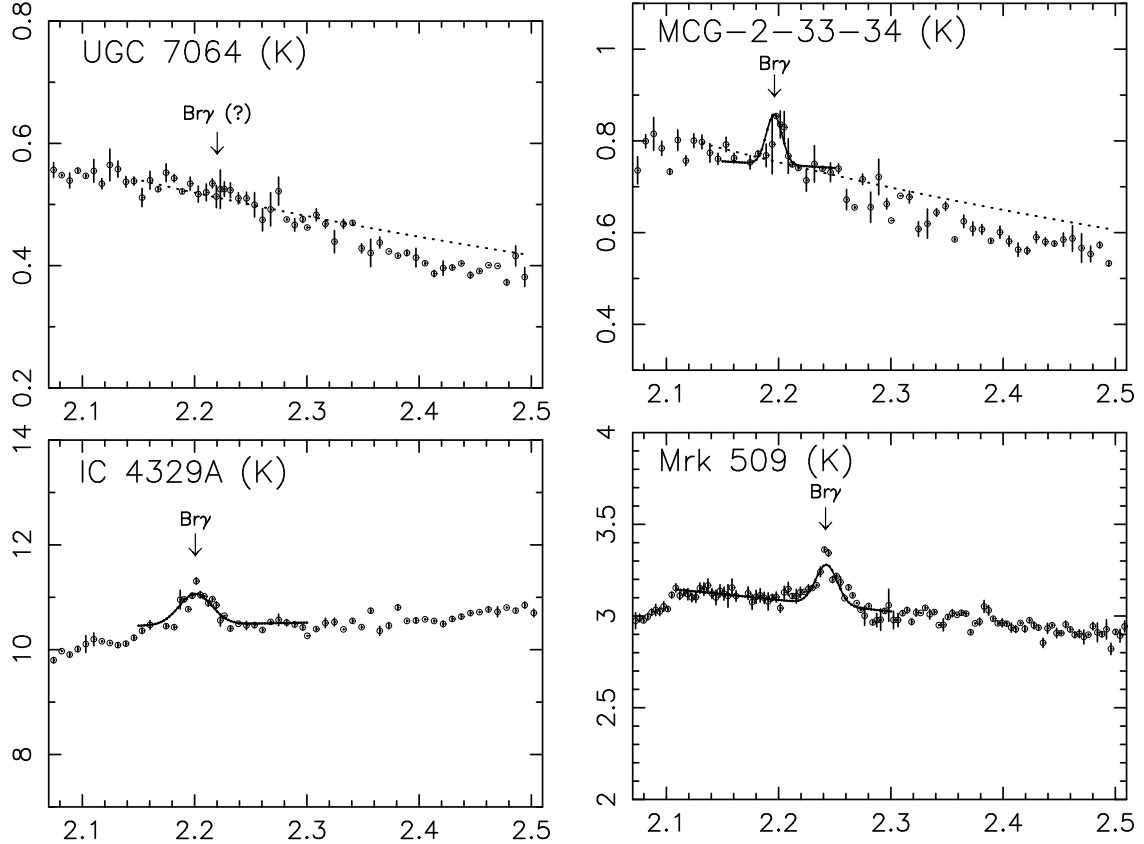
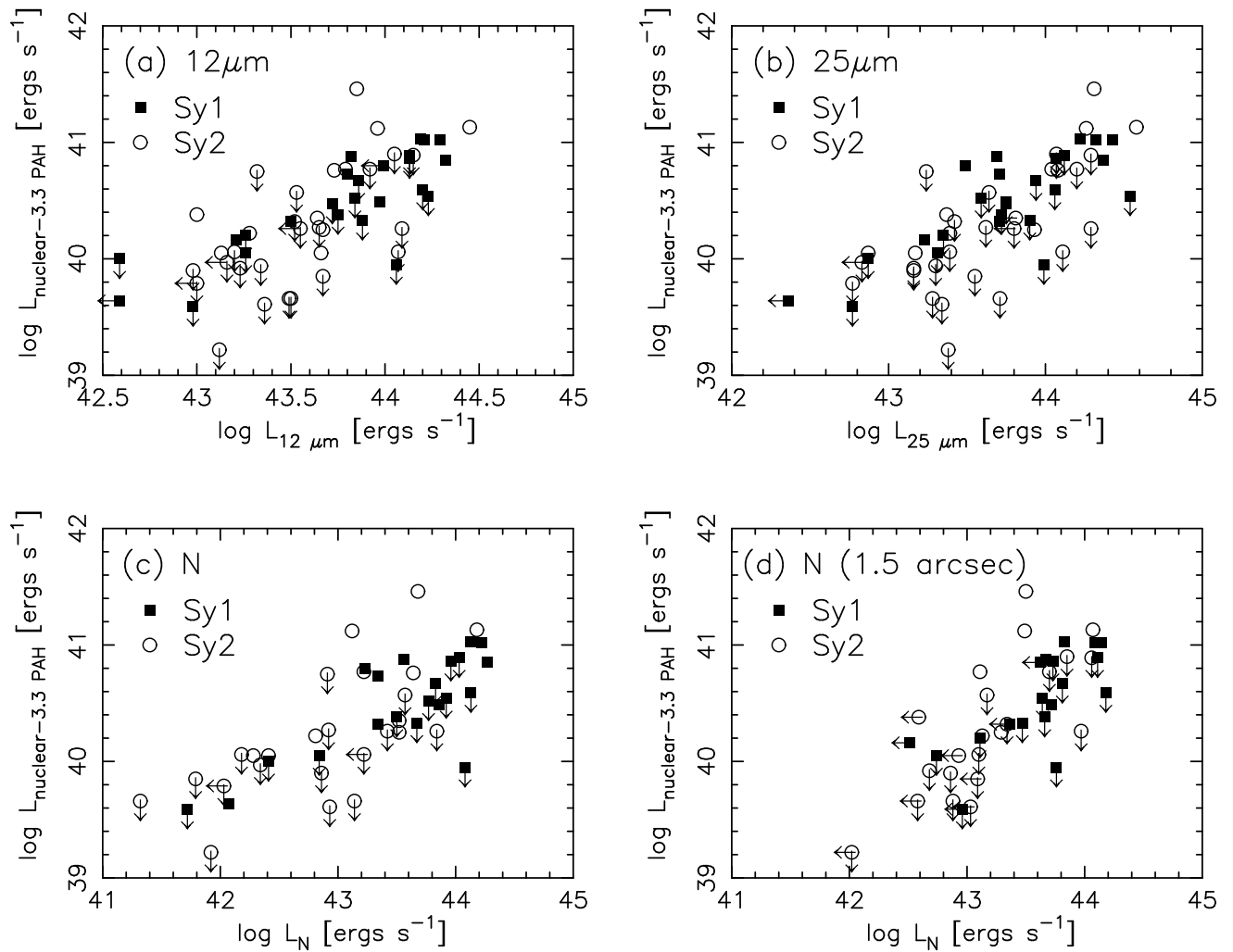


Fig. 2.— Infrared K -band (2.07 – 2.5 μm) slit spectra of the 22 Seyfert 1 nuclei. The abscissa and ordinate are the observed wavelength in μm and F_λ in $10^{-14} \text{ W m}^{-2} \mu\text{m}^{-1}$, respectively. For sources with clear $\text{Br}\gamma$ emission lines, adopted Gaussian fits are overplotted as solid lines. For sources with signatures of CO absorption features, adopted continuum levels, with which to measure the absorption strengths, are shown as dashed lines.



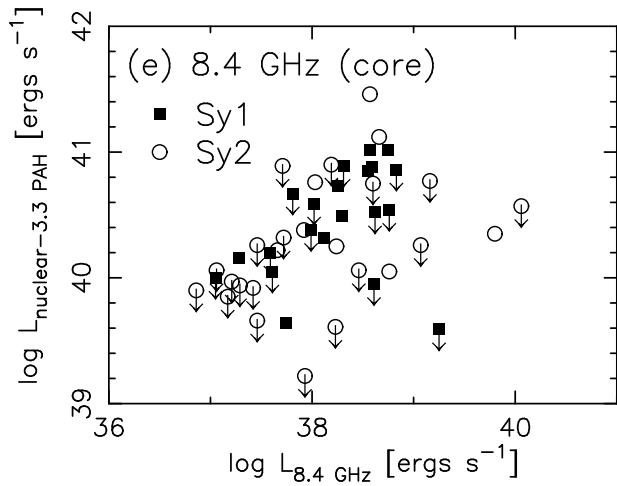


Fig. 3.— (a): Comparison of the *IRAS* 12 μm luminosity, defined as νL_ν (abscissa), and nuclear 3.3 μm PAH emission luminosity detected inside our slit spectra (ordinate). Filled squares are data for Seyfert 1s, and open circles are for Seyfert 2s taken from Imanishi (2003). (b): Same as (a), but the abscissa is *IRAS* 25 μm luminosity. (c): The abscissa is N -band (10.6 μm) luminosity measured with ground-based aperture ($>4''$) photometry, using a single pixel detector. (d): The abscissa is N -band (10.6 μm) luminosity measured with a ground-based two-dimensional camera with a 1''.5 aperture (Gorjian et al. 2004). (e): The abscissa is core radio luminosity at 8.4 GHz measured with 0''.25 spatial resolution (Kukula et al. 1995; Thean et al. 2000). In all the plots, if Seyfert 2s have intrinsically stronger nuclear starbursts, with respect to AGN powers, than Seyfert 1s, their location should be to the upper-left of the Seyfert 1' distribution.

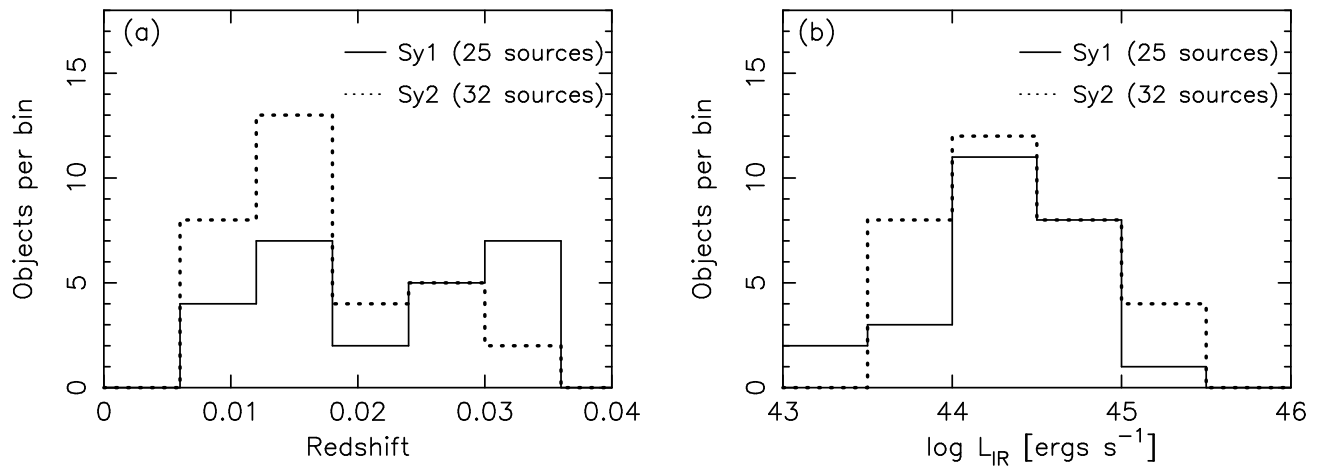


Fig. 4.— (a): Histogram of redshifts. Solid lines are data for Seyfert 1s, and dashed lines are for Seyfert 2s studied by Imanishi (2003). (b): Histogram of the infrared luminosities. For sources that have upper limits in some *IRAS* bands, we assume that the actual flux is the upper limit. For these sources, even though the lower values of infrared luminosities (Table 1) are adopted, there is no systematic difference in the distribution of the infrared luminosities between Seyfert 1s and 2s.

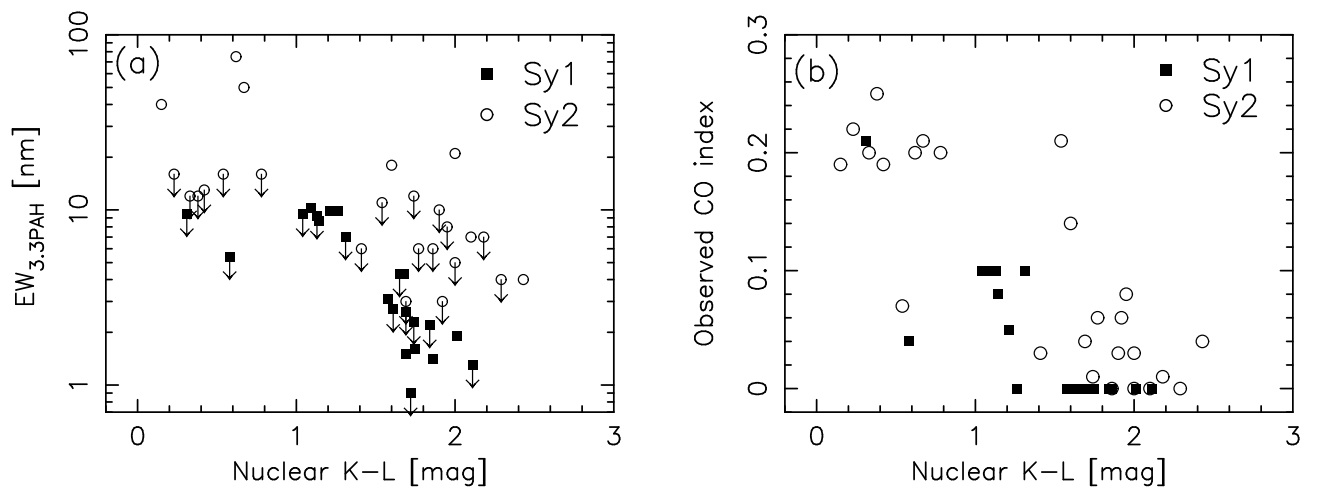


Fig. 5.— (a): Nuclear $K - L$ magnitude (abscissa) and observed rest-frame equivalent width of the $3.3 \mu\text{m}$ PAH emission feature (ordinate). Filled squares are data for Seyfert 1s, and open circles are data for Seyfert 2s adopted from Imanishi (2003). (b): The ordinate is the observed spectroscopic CO index. Filled squares are data for Seyfert 1s, and open circles are for Seyfert 2s taken from Imanishi & Alonso-Herrero (2004).

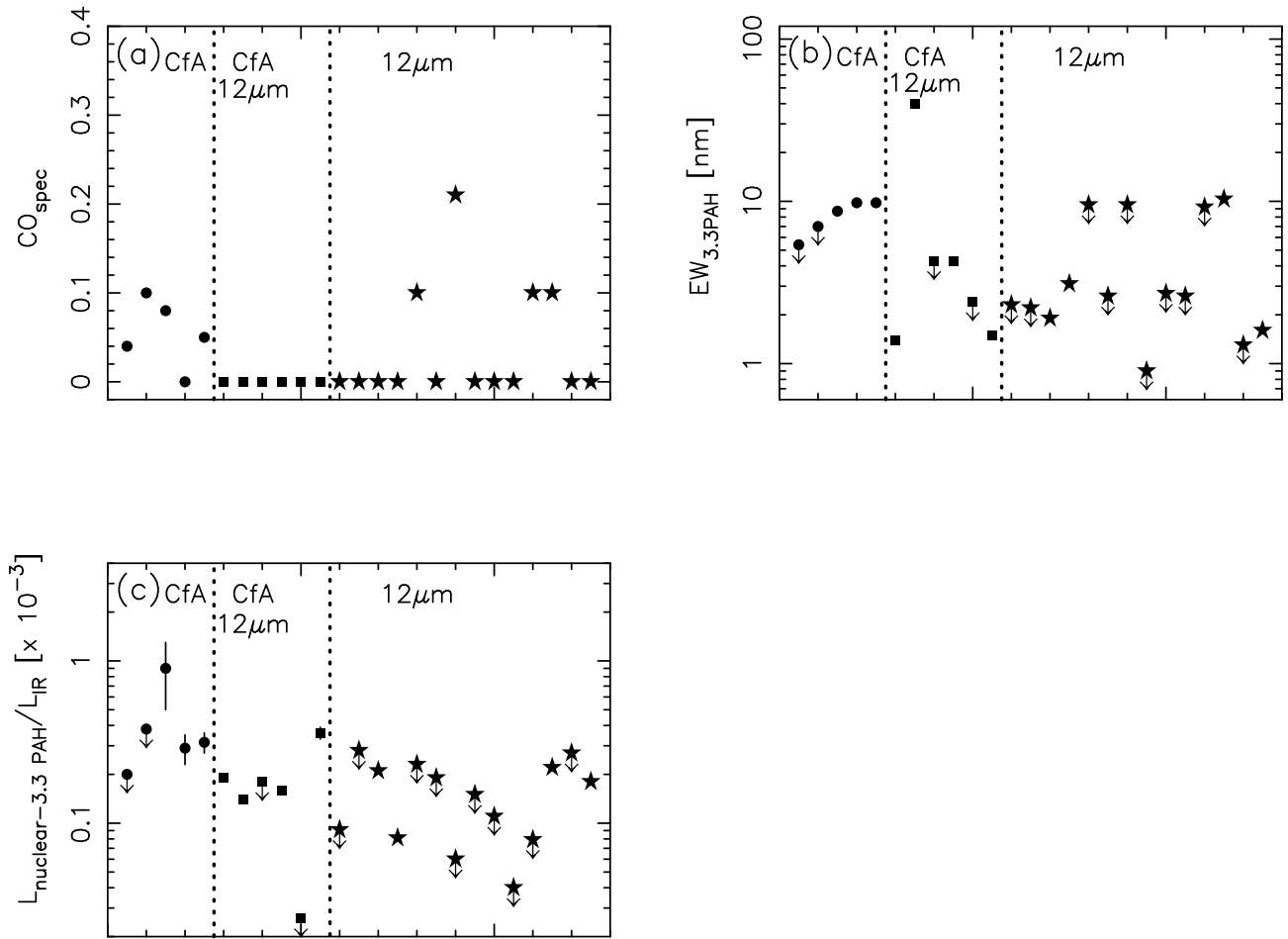


Fig. 6.— (a): Distribution of the observed spectroscopic CO index. Solid circles: CfA Seyfert 1s. Solid stars: 12 μ m Seyfert 1s. Six Seyfert 1s listed in both samples are plotted as solid squares. (b): Rest-frame equivalent width of the 3.3 μ m PAH emission feature. (c): Nuclear 3.3 μ m PAH to infrared luminosity ratio.